

Measurement of transverse momentum relative to dijet systems in PbPb and pp collisions at $\sqrt{s_{NN}} = 2.76$ TeV



The CMS collaboration

E-mail: cms-publication-committee-chair@cern.ch

ABSTRACT: An analysis of dijet events in PbPb and pp collisions is performed to explore the properties of energy loss by partons traveling in a quark-gluon plasma. Data are collected at a nucleon-nucleon center-of-mass energy of 2.76 TeV at the LHC. The distribution of transverse momentum (p_T) surrounding dijet systems is measured by selecting charged particles in different ranges of p_T and at different angular cones of pseudorapidity and azimuth. The measurement is performed as a function of centrality of the PbPb collisions, the p_T asymmetry of the jets in the dijet pair, and the distance parameter R used in the anti- k_T jet clustering algorithm. In events with unbalanced dijets, PbPb collisions show an enhanced multiplicity in the hemisphere of the subleading jet, with the p_T imbalance compensated by an excess of low- p_T particles at large angles from the jet axes.

KEYWORDS: Heavy Ions, Quark gluon plasma, Heavy-ion collision

ARXIV EPRINT: [1509.09029](https://arxiv.org/abs/1509.09029)

Contents

1	Introduction	1
2	CMS detector	3
3	Monte Carlo simulation	4
4	Jet reconstruction	4
5	Track reconstruction	5
6	Analysis	6
6.1	Difference in multiplicities	8
6.2	Transverse momentum balance	8
7	Systematic uncertainties	10
8	Results	14
8.1	Dependence of the p_T balance in pp and PbPb on opening angles around jets	14
8.2	Study of the p_T balance in pp and PbPb collisions, as a function of opening angles around jets in bins of A_J	16
8.3	Dependence of dijet asymmetry on p_T balance and multiplicity difference in jet hemispheres	18
8.4	Dependence of transverse momentum balance on jet distance parameter R	20
9	Summary and conclusions	25
	The CMS collaboration	33

1 Introduction

Partons produced at large transverse momenta (p_T) through hard-scattering processes in heavy-ion collisions are expected to lose energy as they travel through the quark-gluon plasma (QGP) created in these interactions [1]. Experiments at RHIC and the LHC have observed a suppression in the yield of high- p_T particles relative to suitably scaled pp collision data, and a significant reduction in back-to-back high- p_T hadron correlations [2–10] that have been interpreted as evidence for strong partonic interactions within the dense medium that causes the quenching of jets. A direct observation of this effect using jets was provided by ATLAS [11] and CMS [12, 13] through a comparison of the p_T balance of dijets in PbPb and pp collisions. In head-on PbPb collisions, a large increase in asymmetric dijet events was observed relative to the pp reference. This reflects the difference in energy lost

by the two scattered partons in the medium, an effect that becomes more pronounced as the path lengths travelled by the partons and the energy density of the medium increase. In pPb collisions, no excess in unbalanced dijets was observed [14], leading to the conclusion that the dijet imbalance does not originate from initial-state effects. A wide range of models was proposed to accommodate the dependence of dijet data on the jet p_T and the centrality of the collision, i.e. on the degree of overlap of the two colliding nuclei [15–20]. Further evidence for parton energy loss was found in studies of correlations between isolated photons and jets in PbPb events [21], where the unmodified isolated photon provides a measure of the initial parton momentum [22].

As energy is conserved in all interactions in the medium, parton energy loss does not imply the disappearance of energy, but its redistribution in phase space such that it is not recovered with standard jet finding clustering methods. The observed jet quenching naturally leads to questions of how the angular and p_T distributions of charged particles are modified by the energy loss of partons as they traverse the medium. A measurement of these spectra can provide information about the physical processes underlying parton energy loss, which can yield insights into the properties of the strongly interacting medium [23]. Particle distributions inside the jet cone (within $\Delta = \sqrt{(\eta_{\text{trk}} - \eta_{\text{jet}})^2 + (\phi_{\text{trk}} - \phi_{\text{jet}})^2} = 0.2\text{--}0.4$, where ϕ is the azimuthal angle in radians and η is the pseudorapidity) were studied in terms of jet fragmentation functions and jet shapes [24–27]. These distributions show a moderate softening and broadening of the in-cone fragmentation products in PbPb collisions compared to pp data. However, the observed changes account for only a small fraction of the dijet momentum imbalance, indicating that a large amount of energy is transported outside of the jet cone through interactions in the medium.

Identifying the distribution of particle p_T surrounding the jets (i.e. the pattern of p_T “flow” relative to the dijet system) is challenging, as the “lost” p_T is only of the order of 10 GeV, while the total p_T from soft processes forming the underlying event (UE) in a head-on (central) PbPb collision is about three orders of magnitude larger [28, 29]. The angular distribution of the radiated energy is a priori unknown. To overcome these difficulties, CMS previously used the “missing p_T ” method that exploits momentum conservation and azimuthal symmetry in dijet events. This method makes it possible to distinguish the correlated particles carrying the energy lost by jets from the uncorrelated particles, the directions of which are not related to the axes of the jets [12]. The momenta of all charged-particle tracks were therefore projected onto the jet direction, leading to a balancing of the uncorrelated particles, and thereby revealed the p_T flow relative to the dijet system. In pp events, imbalance in the p_T of leading and subleading jets is accommodated through three-jet and multijet final states. In PbPb collisions, quenching effects modify the spectrum and angular distribution of particles that recover the p_T balance within the dijet system. These studies showed that the overall energy balance is restored only when low-momentum particles ($p_T \approx 0.5\text{--}2$ GeV) at large angles to the jet axis ($\Delta > 0.8$) are considered.

The original CMS analysis used a PbPb data sample corresponding to an integrated luminosity of $10 \mu\text{b}^{-1}$ [12], which was insufficient for a detailed study of the angular pattern. In addition, no pp data at the same collision energy was available at the time. In this paper, PbPb data corresponding to an integrated luminosity of $166 \mu\text{b}^{-1}$ from a heavy-ion run

at a nucleon-nucleon center-of-mass energy of 2.76 TeV, and pp data corresponding to an integrated luminosity of 5.3 pb^{-1} taken at the same center-of-mass energy are used in a more comprehensive study. The new data provide an opportunity for detailed characterization of the multiplicity, momentum, and angular distribution of particles associated with the flow of p_T in dijet events in PbPb and pp collisions, as a function of collision centrality and dijet p_T asymmetry. Collision centrality refers to configurations with different impact parameters of the lead nuclei. By changing centrality, the dependence of jet quenching can be studied as a function of the size and density of the medium.

To study the p_T flow relative to the dijet system, two complementary approaches are pursued, both relying on the cancellation of contributions from the uncorrelated UE. First, the p_T of individual tracks are projected onto the dijet axis, defined as the bisector of the leading (highest p_T) jet axis and the subleading (next highest p_T) jet axis, with the latter flipped by π in ϕ . These projections are then summed to investigate the overall p_T flow in dijet events. This “missing p_T ” analysis is used to study how the lost momentum is distributed as a function of the separation of the track from the jet axis, Δ . The second approach involves the study of the difference in the total number of particles emitted in the leading and subleading jet hemispheres. The measurements are carried out as a function of the collision centrality in PbPb collisions, and as a function of the dijet p_T imbalance in pp and PbPb collisions. To investigate how differences in jet fragmentation affect energy loss mechanisms, jets are clustered using several anti- k_T R parameters (0.2, 0.3, 0.4 and 0.5) [30, 31].

2 CMS detector

The central feature of the CMS apparatus is a superconducting solenoid with a 6 m internal diameter. Within the superconducting solenoid volume are a silicon pixel and strip tracker, a lead tungstate crystal electromagnetic calorimeter (ECAL), and a brass and scintillator hadron calorimeter (HCAL), each composed of a barrel and two endcap sections. Forward calorimeters extend the pseudorapidity [32] coverage provided by the barrel and endcap detectors. Muons are measured in gas-ionization detectors embedded in the steel flux-return yoke outside the solenoid.

The silicon tracker measures charged particles within the pseudorapidity range $|\eta| < 2.5$. It consists of 1440 silicon pixel and 15 148 silicon strip detector modules and is located in the 3.8 T field of the superconducting solenoid. For nonisolated particles of $1 < p_T < 10 \text{ GeV}$ and $|\eta| < 1.4$, the track resolutions are typically 1.5% in p_T and 25–90 (45–150) μm in the transverse (longitudinal) impact parameter [33]. The ECAL has coverage up to $|\eta| = 1.48$, and the HCAL up to $|\eta| = 3$. Steel and quartz fibre hadron forward (HF) calorimeters extend the acceptance to $|\eta| = 5$. For central η , the calorimeter cells are grouped in projective towers of granularity $\Delta\eta \times \Delta\phi = 0.087 \times 0.087$. The ECAL was initially calibrated using test beam electrons, and then with photons from π^0 and η meson decays and electrons from Z boson decays [34–36]. The energy scale in data agrees with that in the simulation to better than 1 (3)% in the barrel (endcap) region, $|\eta| < 1.5$ ($1.3 < |\eta| < 3.0$) [37]. Hadron calorimeter cells in the $|\eta| < 3$ region are calibrated primarily with

test beam data and radioactive sources [38, 39]. A more detailed description of the CMS detector, together with a definition of the coordinate system and kinematic variables, can be found in ref. [32].

3 Monte Carlo simulation

To study the performance of jet reconstruction in PbPb and pp collisions, dijet events in nucleon-nucleon collisions are simulated with the PYTHIA Monte Carlo (MC) event generator [40] (version 6.423, tune Z2¹ [41]). To account for isospin effects present in PbPb collisions, the underlying pp, pn, and nn subcollisions are weighted by cross sections using the model from ref. [42]. For the simulation of dijet signals, a minimum hard-interaction scale of 30 GeV is used to increase the number of dijet events.

To model the PbPb UE, minimum bias PbPb events are simulated with the HYDJET event generator, version 1.8 [42]. The parameters of this version are tuned to reproduce total particle multiplicities, improve agreement with the observed charged-hadron spectra, and to approximate the fluctuations in UE seen in data. Proton-proton collisions are generated using leading-order (LO) PYTHIA (without HYDJET simulation). Full detector simulation using the GEANT4 package [43] and the standard CMS analysis chain are used to process both PYTHIA dijet events and PYTHIA dijet events embedded into HYDJET events (denoted PYTHIA+HYDJET in this paper).

Jet reconstruction is studied using the jet information in the PYTHIA generator in comparison to the same fully reconstructed jet in PYTHIA+HYDJET, after matching the generator-level and reconstructed jets in angular regions of $\Delta^{\text{reco,gen}} = \sqrt{(\eta_{\text{jet}}^{\text{gen}} - \eta_{\text{jet}}^{\text{reco}})^2 + (\phi_{\text{jet}}^{\text{gen}} - \phi_{\text{jet}}^{\text{reco}})^2} < R$.

4 Jet reconstruction

Jet reconstruction in heavy-ion collisions at CMS is performed using the anti- k_T algorithm and distance parameters $R = 0.2$ through 0.5 , encoded in the FastJet framework [30]. Jets are reconstructed based on energies deposited in the CMS calorimeters. The probability of having a pileup collision is 23%, and the average transverse energy (E_T) associated with the UE is less than 1 GeV. For pp collisions, no subtraction is employed for the underlying event (UE) nor for pileup from overlapping pp interactions. Whereas, for PbPb collisions, a new ‘‘HF/Voronoi’’ algorithm is used to subtract the heavy-ion background [44]. The transverse energy is defined by $E_T = \sum E_i \sin(\theta_i)$, where E_i is the energy of the i^{th} particle in the calorimeter, θ_i is the polar angle of particle i measured from the beam axis, and the sum is over all particles emitted into a fixed Δ in an event.

The HF/Voronoi algorithm removes the UE contribution by estimating the E_T contribution from the UE at central η , and its azimuthal dependence, from deposition in the HF detector. The estimation is performed using a polynomial model that is trained using a singular-value decomposition method [45], separately on minimum bias data and

¹The PYTHIA6 Z2 tune is identical to the Z1 tune described in [41], except that Z2 uses the CTEQ6L PDF, while Z1 uses CTEQ5L.

MC simulation. After an average E_T is subtracted from each calorimeter tower, based on its location in η and ϕ , the calorimeter towers containing non-physical negative E_T are evened out by redistributing the energy in neighboring positive E_T towers in a circular region of the parameter $R+0.1$. The redistribution is implemented by minimizing a metric that describes the total energy difference before and after the process, given that after the redistribution all towers have positive energy.

The initial calorimetric E_T values are corrected as a function of p_T and η to match the jets clustered using all particles, except neutrinos, at the generator level of PYTHIA. The consistency of the corrected jet energy scale (JES), defined as $\langle p_T^{\text{reco}}/p_T^{\text{gen}} \rangle$, is checked as a function of p_T and η using PYTHIA+HYDJET events in bins of event centrality. The deviations are within 2% for all centrality, p_T , and η bins, and less than 1% for jet p_T greater than 60 GeV.

The nonlinear response of the calorimeter as a function of particle energy gives jets that fragment into many particles with smaller energies a smaller response relative to the jets of same energy but with fewer fragments. To account for the dependence of JES on the fragmentation of jets, an additional correction is applied as a function of reconstructed jet p_T , and as a function of the number of charged particles with $p_T > 2$ GeV in a cone of R around the jet axis. The number of charged particles in PYTHIA+HYDJET is calculated using the p_T values obtained after the “HF/Voronoi” subtraction. For PYTHIA, p_T values without any UE subtraction are used to calculate the number of charged particles. The fragmentation-dependent correction applied in PbPb collisions is calculated using PYTHIA+HYDJET events with matching UE activity. This correction results in a reduction in separation of the JES for quark and gluon jets, and also lessens the impact of jet reconstruction on fragmentation of the leading and subleading jets.

The residual JES that accounts for the difference in calorimeter response in data and MC events is calculated using dijet balance in pp and peripheral (50–100% centrality) PbPb collisions [46], based on data. This difference is found to be less than 2% for $|\eta| < 2$.

5 Track reconstruction

For studies of pp data and PYTHIA MC events, charged particles are reconstructed using the same iterative method [33] as in previous CMS analyses of pp collisions. However, for PbPb data and PYTHIA+HYDJET events, a different iterative reconstruction [8, 25] is employed after extending the global tracking information down to $p_T = 0.4$ GeV. To minimize the impact of inefficiencies in track reconstruction caused by the p_T resolution in track seeds near the 0.4 GeV threshold, only tracks with $p_T > 0.5$ GeV are used in this analysis.

Reconstructed tracks in PYTHIA and PYTHIA+HYDJET simulations are matched to primary particles using the associated hits, i.e., charged particles that are produced in the interaction or are remnants of particles with a mean proper lifetime of less than 5×10^{13} GeV⁻¹. The misidentification rate is defined as the fraction of reconstructed tracks that do not match any charged particle (primary or otherwise). The multiple reconstruction rate is given by the fraction of primary particles that are matched to more than one reconstructed track. Tight track quality criteria are applied to reduce the rate of

misidentified or secondary particles [33]. Requirements are less restrictive for pp than for PbPb collisions. Heavy-ion tracking requires a larger number of hits in the tracker and a smaller normalized fit χ^2 value for fits to reconstructed tracks. For both systems, tracks are required to be compatible with the vertex with the largest value in the sum of their p_T .

In pp collisions, the track reconstruction efficiency is $\approx 90\%$ at $p_T = 10$ GeV and 80% at 0.5 GeV. The misidentification rate for tracks is $< 2\%$ for $p_T > 1$ GeV and slightly higher below this value. The contribution from secondary particles is subtracted, as the secondary-particle rate is as high as 2% . The multiple reconstruction rate is smaller than 1% . The efficiency and misidentification corrections are calculated as a function of η , ϕ , p_T , and the distance to the nearest jet axis, while simpler secondary-particle and multiple reconstruction corrections are applied that depend only on the η and p_T values of charged particles.

As the track reconstruction efficiency in pp collisions is larger than in PbPb collisions, the momentum flow can be measured with higher precision, while in the high-multiplicity environment of heavy-ion collisions track reconstruction remains a challenge. In PbPb collisions, the reconstruction efficiency for primary charged particles, after implementing the above track quality criteria, is approximately 70% at $p_T \approx 10$ GeV. Efficiency starts to drop for p_T below 5 GeV and at 0.5 GeV the efficiency is 30% . The misidentification rate for tracks with $p_T = 0.5$ GeV is $\approx 35\%$, but decreases to values smaller than 2% and for $p_T > 1$ GeV. The secondary-particle rate and multiple-reconstruction rate are, respectively, less than 0.5% and 0.3% over the whole p_T range in the analysis. No corrections are applied for these in PbPb collisions. Using PYTHIA+HYDJET simulations, track reconstruction efficiency and misidentification rates are evaluated as a function of the η , ϕ , and p_T of the track, as well as the centrality of the collision, and the smallest distance in Δ between the track and a jet with $p_T > 50$ GeV.

Tracks used in the analysis are weighted with a factor to correct for the effects described above. The value of this correction is

$$c^{\text{trk}} = \frac{(1 - \text{misreconstruction})(1 - \text{secondary-particle})}{(\text{efficiency})(1 + \text{multiple-reconstruction})}, \quad (5.1)$$

where secondary-particle and multiple-reconstruction rates are set to zero for PbPb collisions.

6 Analysis

Events are selected using an inclusive single-jet trigger with jet $p_T > 80$ GeV. To suppress electronic noise, cosmic rays, and beam backgrounds, events are required to satisfy selection criteria documented in refs [12, 21]. Events passing selections are subject to offline jet reconstruction. To select samples containing high- p_T dijets, events are required to have a leading (subleading) jet in the range of $|\eta| < 2$ with a corrected jet $p_T > 120$ (50) GeV. The single-jet trigger is fully efficient for events with the requirement on the leading jet p_T for all the R parameters in the analysis. To select a dijet topology, the azimuth between the leading and subleading jets is required to be $\Delta\phi_{1,2} = |\phi_1 - \phi_2| > 5\pi/6$. Once leading

and subleading jets are identified within the initial range of $|\eta| < 2$, both jets are then restricted to be within a tighter $|\eta|$. For measurements that offer comparison to a previous analysis [12], we use the previous selection of $|\eta| < 1.6$. For those that extend up to large angular distances Δ , a tighter requirement of $|\eta| < 0.6$ is applied, such that leading and subleading jets are far from the edge of the tracker and all ranges in Δ fall within the acceptance.

This analysis aims to provide information that would aid the characterization of the energy loss mechanisms responsible for the increase in the fraction of unbalanced dijet pairs in central PbPb relative to pp collisions. As hard-scattered partons travel and shower in the QGP, they can both trigger a coherent medium response and undergo interactions in the medium that modify the showers of both partons. However, the enhancement in unbalanced dijet pairs suggests that, on average, the subleading jet loses more energy than the leading jet. The modification in jet balance must be compensated by the remaining, unclustered constituents of the event, as each interaction conserves overall momentum.

The particles that provide the p_T balance are correlated with the jet axes, but the particles that are not affected by the interaction of the partons with the medium are evenly distributed in azimuth relative to the individual directions of the leading and subleading jets. The total p_T of these particles is uncorrelated with the dijet pair. To differentiate the uncorrelated and correlated particles, we compare differences in multiplicity in leading and subleading jet hemispheres. In addition, we measure modifications in the p_T spectrum of charged particles that contribute to the overall p_T balance in the event, as well as their angular distribution with respect to the dijet system. Using the azimuthal symmetry of the jet axes relative to the UE makes it possible to perform precise measurements for particles down to $p_T = 0.5$ GeV, and angles as large as $\Delta = 1.8$. This provides constraints on energy loss mechanisms despite the small signal-to-background ratio.

The cancellation of the uncorrelated UE depends on azimuthal symmetry of the areas selected around the leading and subleading jets relative to the axis of projection. As mentioned above, to ensure this requirement, the dijet azimuthal angle (ϕ_{dijet}) is defined as the average ϕ of the leading and subleading jets after the subleading jet is reflected around the origin. In contrast with previous publications [12], ϕ_{dijet} is preferred over ϕ_1 (the ϕ of the leading jet) for the projection axis, because the latter choice breaks azimuthal symmetry, by generating particles near the leading jet that have larger projections at small angles relative to particles produced at the same distance to the subleading jet.

The perfect cancellation of contributions from particles to p_T flow, and to differences in hemisphere multiplicities from UE, take place only when there is no interaction between UE and the jets. This is the case in PYTHIA+HYDJET simulations. In data, due to the variations in path length in medium traversed by jets there are complicated correlations between particles from different interactions and jet directions. These correlations comprise a part of the signal probed in this analysis.

The observables used in this analysis are measured in bins of centrality and dijet imbalance. The dependence on centrality in PbPb collisions is investigated in terms of the emergence and enhancement of jet quenching effects as the size of the medium and energy density increase, and the dijet imbalance enriches events with subleading jets that lose more

energy than the leading jet. To define centrality classes, collisions with inelastic hadronic interactions are divided into percentages according to the E_T of calorimeter towers summed in the HF, and events are assigned into classes of centrality based on these total sums in the HF. The distribution in this E_T is used to divide the event sample into bins, each representing 0.5% of the total nucleus-nucleus interaction cross section. Following refs. [12, 13], we quantify p_T imbalance through the asymmetry ratio $A_J = (p_{T,1} - p_{T,2}) / (p_{T,1} + p_{T,2})$, where $p_{T,1}$ and $p_{T,2}$ are the p_T of the leading and subleading jets within $\eta < 2.0$, respectively. The A_J boundaries used in the analysis are 0.11, 0.22, 0.33 and 0.44, which correspond to $p_{T,2}/p_{T,1}$ values of 0.8, 0.64, 0.50 and 0.42, respectively.

6.1 Difference in multiplicities

The events are bisected with a plane perpendicular to ϕ_{dijet} into two hemispheres associated with the leading and subleading jets. The multiplicity difference is defined as the difference between the corrected number of tracks with $p_T > 0.5$ GeV ($N_{\text{trk}}^{\text{Corrected}} = \sum c^{\text{trk}}$) in these two hemispheres:

$$\Delta_{\text{mult}} = N_{\text{trk}}^{\text{Corrected}}|_{|\phi_{\text{trk}} - \phi_{\text{dijet}}| > \pi/2} - N_{\text{trk}}^{\text{Corrected}}|_{|\phi_{\text{trk}} - \phi_{\text{dijet}}| < \pi/2}. \quad (6.1)$$

Positive Δ_{mult} means that an excess of particles is found in the hemisphere of the subleading jet, relative to the number of particles in the leading jet hemisphere. This quantity is measured event-by-event and then averaged in bins of the observables of interest. It is sensitive to the number of jets in a given hemisphere and their fragmentation, as well as to the additional particles produced in jet quenching or through some specific response of the QGP medium in one of the two hemispheres.

To select events that show consequences of jet quenching, the measurement is carried out as a function of A_J and collision centrality. The A_J -dependent measurement is performed for jets with a distance parameter of $R = 0.3$.

To see modifications in the p_T spectrum associated with the difference in multiplicities in two hemispheres, Δ_{mult} is measured for track p_T ranges of 0.5–1, 1–2, 2–4, 4–8, and 8–300 GeV, and divided by the bin width. The measurement is repeated for different R parameters.

To be consistent with the measurement of p_T balance, the leading and subleading jets used in the A_J -dependent Δ_{mult} measurement are required to fall in the pseudorapidity region of $|\eta| < 1.6$. The leading and subleading jets used in the R -dependent measurement are required to be within $|\eta| < 0.6$. Although in both cases jets with $|\eta| > 2$ are excluded, it is important to note that starting jet reconstruction with a cutoff $|\eta| < 1.6$, (or < 0.6) is different than using the $|\eta| < 2$ selection for determining the highest- p_T jets and then applying a tighter requirement, since events in which the leading or subleading jets are found in the range between $|\eta| = 1.6$ (or 0.6) and $|\eta| = 2.0$ are also excluded.

6.2 Transverse momentum balance

Detailed information about the p_T flow relative to the dijet system can be obtained by studying the contribution of tracks to the overall p_T balance in the event, as characterized

by individual track p_T and angle relative to the jets. To calculate the p_T balance, the p_T of tracks are projected onto the dijet axis. For each track, this projection is defined as

$$p_T^{\parallel} = -c^{\text{trk}} p_T^{\text{trk}} \cos(\phi_{\text{trk}} - \phi_{\text{dijet}}), \quad (6.2)$$

where, as mentioned in section 5, the correction for reconstruction effects accounts for the misreconstruction rate and reconstruction efficiency for PbPb collisions, with values specified by eq. (5.1). In addition, secondary particle and multiple reconstruction rates are corrected in pp collisions.

Particles that make a positive contribution in Δ_{mult} also have positive p_T^{\parallel} , as the cosine function changes sign at $\pi/2$. These two observables therefore map onto each other with a weight in track p_T and $\cos(\phi_{\text{trk}} - \phi_{\text{dijet}})$.

To study the angular recovery rate (rate at which imbalance is restored, as momentum contributions are included further from the jet cone) and the associated spectra of p_T balance, tracks that fall in annular regions around the jet axes are grouped together according to their p_T . In each event, p_T^{\parallel} values of these group of tracks are summed to obtain \not{p}_T^{\parallel} . For each region, \not{p}_T^{\parallel} is calculated in track p_T ranges of 0.5–1, 1–2, 2–4, 4–8, and 8–300 GeV. Annular regions are defined in $\Delta = \sqrt{(\phi_{\text{trk}} - \phi_{\text{jet}})^2 + (\eta_{\text{trk}} - \eta_{\text{jet}})^2}$ and binned between $\Delta = 0.0$ –1.8 in steps of 0.2. In addition, the contribution from charged particles that fall outside of this range are all collected in an extra overflow bin. These particles lie in the range of $1.8 < \Delta < 3.6$, depending on the η of the dijet pair. No anti- k_T clustering is employed in the calculation of Δ , and tracks are defined to lie within circular regions in pseudorapidity and azimuth. The axes used to define the annuli differ from the projection axis, ϕ_{dijet} . For large Δ , the annuli around the leading and subleading jets can overlap, in which case, the track used in the overlap region when calculating \not{p}_T^{\parallel} , is the one in the annulus at smaller radius. The overlaps do not occur before $\Delta = 5\pi/12$.

The \not{p}_T^{\parallel} is averaged over events with a specific A_J value separately for pp and PbPb collisions, and for PbPb collisions they are divided into classes of collision centrality. This average is denoted as $\langle \not{p}_T^{\parallel} \rangle_{p_T^{\text{trk}}, \Delta}$, to indicate that within each event the balance is calculated using a subset of tracks with specific Δ and p_T .

Using the track p_T and Δ parameters limits the selections on collision centrality and A_J because of the statistical imprecision of the data. For more detailed analysis of the dependance of track p_T on event properties, Δ binning can be removed by adding up the $\langle \not{p}_T^{\parallel} \rangle_{p_T^{\text{trk}}, \Delta}$ values for each Δ bin, which is identical to not having annular requirements in the first place, to obtain

$$\langle \not{p}_T^{\parallel} \rangle_{p_T^{\text{trk}}} = \sum_{\Delta} \langle \not{p}_T^{\parallel} \rangle_{p_T^{\text{trk}}, \Delta}. \quad (6.3)$$

The p_T balance, as in eq. (6.3), calculated for tracks in a given p_T range usually yields nonzero values, because of the differences in p_T spectra of particles in subleading jet hemisphere relative to the spectra in the leading jet hemisphere. Summing the signed $\langle \not{p}_T^{\parallel} \rangle_{p_T^{\text{trk}}}$ values for each track p_T bin provides an overall p_T balance in the event for tracks with $0.5 < p_T < 300$ GeV, that takes values close to zero, because of momentum conservation. There can still be a deviation from zero because of the particles with $p_T <$

0.5 GeV, as well as for those particles that fall out of the tracker coverage in pseudorapidity that are not included in the measurement. This sum corresponds to

$$\langle \cancel{p}_T^{\parallel} \rangle_{\Sigma} = \sum_{p_T^{\text{trk}}} \langle \cancel{p}_T^{\parallel} \rangle_{p_T^{\text{trk}}}. \quad (6.4)$$

The angular distribution of p_T balance is studied differentially in bins of track p_T by $\langle \cancel{p}_T^{\parallel} \rangle_{p_T^{\text{trk}}, \Delta}$, as described above, and adding up the contribution from different track p_T bins gives

$$\langle \cancel{p}_T^{\parallel} \rangle_{\Delta} = \sum_{p_T^{\text{trk}}} \langle \cancel{p}_T^{\parallel} \rangle_{p_T^{\text{trk}}, \Delta}, \quad (6.5)$$

which defines the contribution of all tracks with $0.5 < p_T < 300$ GeV in a given annulus to total p_T balance. This $\langle \cancel{p}_T^{\parallel} \rangle_{\Delta}$, summed over all Δ intervals, yields $\langle \cancel{p}_T^{\parallel} \rangle_{\Sigma}$. Instead of summing all Δ bins, to calculate the recovery of balance as radius gets larger, the annuli can be summed from $\Delta = 0$ up to the angle of interest, and a cumulative balance inside a cone calculated, as

$$\langle \cancel{p}_T^{\parallel} \rangle_{[0, \Delta]} = \sum_{\Delta'=0}^{\Delta'= \Delta} \langle \cancel{p}_T^{\parallel} \rangle_{\Delta'}. \quad (6.6)$$

As mentioned previously, for consistency with the analysis in ref. [12], in calculations that integrate over Δ , e.g. for, $\langle \cancel{p}_T^{\parallel} \rangle_{p_T^{\text{trk}}}$ and $\langle \cancel{p}_T^{\parallel} \rangle_{\Sigma}$, only events in which both leading and subleading jets fall within $|\eta| < 1.6$ are included in the measurement of p_T balance. For measurements where contributions of different annuli are studied, to ensure full tracker coverage around jets over $\Delta < 1.8$ for $\langle \cancel{p}_T^{\parallel} \rangle_{p_T^{\text{trk}}, \Delta}$, $\langle \cancel{p}_T^{\parallel} \rangle_{\Delta}$, and $\langle \cancel{p}_T^{\parallel} \rangle_{[0, \Delta]}$, tighter restrictions are required on the pseudorapidity of leading and subleading jets ($|\eta| < 0.6$) after they are found within $|\eta| < 2$.

7 Systematic uncertainties

The sources of major systematic uncertainty can be categorized into two groups; biases related to jet reconstruction and those related to track reconstruction. Effects associated with event selection and beam background rejection are found to be negligible.

The biases related to jet reconstruction are caused by smearing of jet p_T due to energy resolution and uncertainties in the JES. These factors can change the p_T -ordering of jets in the event, resulting in the interchanging of leading and subleading jets, or causing third jet to replace the subleading jet. The uncertainties are estimated as a function of centrality and A_J in each charged-particle p_T range, using PYTHIA and PYTHIA+HYDJET simulations to compare observables calculated with reconstructed jets to generator-level jets. A bin-by-bin correction is applied to data to account for the observed jet reconstruction bias. This uncertainty includes the effect of jet-angular resolution. However, the size of the bins in the Δ -dependent measurement is significantly larger than a typical angular resolution, which therefore has a negligible effect on the observables. Going from $R = 0.2$ to 0.5 , the angular resolution, defined by the standard deviation of the $\Delta^{\text{reco,gen}}$ distribution, increases from 0.020 to 0.025 for leading jets, and from 0.025 to 0.035 for subleading jets in pp. The

	Values integrated over A_J					
	pp		PbPb, 30–100%		PbPb, 0–30%	
Δ	<0.2	0.2–2.0	<0.2	0.2–2.0	<0.2	0.2–2.0
Jet reconstruction	<1	0.0–0.2	1	0.1–0.2	1	0.1–0.4
Data/MC differences for JES	1	0.1–0.2	2	0.1–0.3	2	0.1–0.3
Fragmentation dependent JES	<1	0.1–0.2	2	0.1–0.2	1	0.1–0.4
Track corrections	<1	<0.1	1	0.0–0.2	2	0.2–0.9
Data/MC differences for tracking	1	0.0–0.1	1	0.1–0.2	1	0.1–0.2
Total	1	0.1–0.3	2	0.2–0.3	3	0.2–1.0

	$A_J < 0.22$					
	pp		PbPb, 30–100%		PbPb, 0–30%	
Δ	<0.2	0.2–2.0	<0.2	0.2–2.0	<0.2	0.2–2.0
Jet reconstruction	<1	0.1–0.2	1	0.1–0.2	1	0.1–0.4
Data/MC differences for JES	1	0.1–0.2	2	0.1–0.4	2	0.2–0.4
Fragmentation dependent JES	<1	0.1	2	0.1–0.4	1	0.1–0.5
Track corrections	<1	<0.1	1	0.1	2	0.1–0.6
Data/MC differences for tracking	<1	0.0–0.1	1	0.1	1	0.1
Total	1	0.1–0.3	2	0.2–0.4	3	0.2–0.6

	$A_J > 0.22$					
	pp		PbPb, 30–100%		PbPb, 0–30%	
Δ	<0.2	0.2–2.0	<0.2	0.2–2.0	<0.2	0.2–2.0
Jet reconstruction	2	0.1–0.5	1	0.1–0.6	2	0.2–0.6
Data/MC differences for JES	2	0.1–0.3	3	0.2–0.5	3	0.3–0.6
Fragmentation dependent JES	1	0.1–0.5	1	0.1–0.7	1	0.2–0.6
Track corrections	<1	0.1	1	0.1–0.3	3	0.2–1.1
Data/MC differences for tracking	2	0.1–0.2	2	0.1–0.2	2	0.1–0.3
Total	3	0.3–0.8	3	0.3–0.9	4	0.4–1.4

Table 1. Systematic uncertainties in $\langle p_T^\parallel \rangle_\Delta$ for jets clustered with distance parameter of 0.3 in pp, and in central and peripheral PbPb collisions, for different A_J selections. Uncertainties are shown as shifts in the values in units of GeV (rather than as fractions) for two Δ selections.

same holds in 30–100% centrality PbPb collisions. In the most central 0–30% of events, the corresponding ranges are 0.020–0.035 and 0.025–0.045, respectively.

After implementing the fragmentation-dependent jet energy corrections there is up to 5% difference between the JES for quark and gluon jets at $p_T < 50$ GeV, and the difference disappears for high- p_T jets. Additional checks are therefore pursued to account for possible discrepancies in the performance of jet energy corrections in data and in MC simulations.

A modification in flavor content of jets due to quenching can lead to an under- or over-correction of the jet energy in data. Also, the uncertainty in the JES from differences in simulation and detector conditions is calculated to be 2% using a data-based “tag-and-probe” technique that depends on dijet balance in a control sample of peripheral PbPb events [46]. The jet p_T is changed up and down for leading and subleading jets in an asymmetric manner (leading JES is increased while subleading JES is decreased) as a function of jet p_T , to account for the differences in JES between quark and gluon jets and the data-based JES uncertainty. Because the number of charged particles is a parameter in these corrections, and can make the fragmentation-dependent jet energy corrections sensitive to quenching effects, the difference in the observables before and after corrections in MC events is compared to the corresponding change in data, and the discrepancy between data and simulation is quoted as an additional source of uncertainty.

Uncertainties related to track reconstruction are calculated in PYTHIA and PYTHIA+HYDJET by comparing the results with generator-level charged particles to those with reconstructed tracks, after applying the track corrections discussed in section 5. The small uninstrumented regions in the detector, and the correlation between track reconstruction efficiency and JES are the main causes of discrepancies observed between results with generator-level particles and reconstructed tracks. The track corrections account for the inefficiencies due to uninstrumented regions. However, the bins used in η and ϕ to calculate the reconstruction efficiency are larger than the size of the uninstrumented regions, and as a result cannot completely correct the effect of these. An additional uncertainty is therefore added to account for the effect of differences in detector conditions and simulation of track reconstruction. This is achieved using the ratio of corrected to initial track p_T and η spectra in data and simulations that are compared as track-quality selections are changed. The difference is found to be less than 5%, which is included in the systematic uncertainty.

To calculate the total uncertainty, the uncertainties from sources mentioned above are summed in quadrature. The contribution of each item is summarized in tables 1–3 for the $\langle \not{p}_T^\parallel \rangle_\Delta$ measurement. The systematic sources are given in terms of shifts in the value of each observable in a given bin in units of GeV instead of % changes, as the $\langle \not{p}_T^\parallel \rangle_\Delta$ can vanish and can take values arbitrarily close to zero. Typically, $\langle \not{p}_T^\parallel \rangle_\Delta$ is between 15–40 GeV near the jet axes ($\Delta < 0.2$), and less than 10 GeV at larger angles.

The dependence of uncertainties in dijet asymmetry and centrality is summarized in table 1 for jets with a distance parameter $R = 0.3$. The jet energy resolution, can cause events to move across the A_J boundaries. Moreover, it is more likely for the leading jet in a highly imbalanced dijet event to be located in a region of an upward UE fluctuation in PbPb collisions. For these reasons, uncertainties related to jet reconstruction are larger in imbalanced dijet events. For well-balanced events, the uncertainty is comparable to that in the inclusive A_J selection, because the increase in effects from jet energy resolution balances the reduction of effects related to UE fluctuations. Uncertainties in track reconstruction are larger in imbalanced than in balanced events, because of the correlation of track reconstruction efficiency and reconstructed jet energy. When a high- p_T track that carries a significant fraction of jet p_T is not reconstructed, the jet energy is under-corrected, and

	0.5 < p _T < 2 GeV		2 < p _T < 8 GeV		p _T > 8 GeV	
Δ	<0.2	0.2–2.0	<0.2	0.2–2.0	<0.2	0.2–2.0
Jet reconstruction	0.04	0.06–0.25	0.13	0.04–0.14	0.85	0.01–0.07
Data/MC differences for JES	0.14	0.07–0.24	0.42	0.03–0.11	0.97	0.01–0.12
Fragmentation dependent JES	0.03	0.10–0.14	1.1	0.05–0.23	0.19	0.02–0.06
Track corrections	0.09	0.08–0.64	0.27	0.06–0.13	1.78	0.01–0.07
Data/MC differences for tracking	0.04	0.03–0.08	1.2	0.01–0.05	1.16	0.00–0.02
Total	0.17	0.20–0.69	1.1	0.11–0.29	2.3	0.04–0.10

Table 2. Systematic uncertainties in $\langle p_T^\parallel \rangle_{p_T^{\text{trk}}, \Delta}$ in 0–30% PbPb collisions, for jets clustered with a distance parameter of 0.3, as a function of charged-particle p_T . Uncertainties are shown as shifts in the values in units of GeV (rather than as fractions) for two Δ selections.

vice versa, the energy is over-corrected in events where the high- p_T track is found, because jet energy corrections are obtained for the average case where the high- p_T track might not be reconstructed. Events with highly imbalanced dijets can result from miscalculated jet energies caused by inefficiencies in track reconstruction. Centrality of PbPb collisions does not affect the uncertainties within the jet cone as much as at larger angles, where the signal-to-background ratio gets smaller. Track and jet reconstruction uncertainties, caused by over-correction of the leading jet p_T because of upward UE fluctuations, in particular, tend to increase in central collisions. Uncertainties are smaller in pp than in PbPb collisions because of the absence of a heavy-ion UE, and differences in jet and track reconstruction that provide better measurement of jet p_T , larger track reconstruction efficiency, and lower track misidentification rates.

Uncertainties for small Δ are dominated by charged particles with $p_T > 8$ GeV, while at larger Δ , low- p_T particles make up a larger fraction of the total uncertainty in events when there is no selection made on charged-particle p_T . The contribution from each range of track p_T to the uncertainty in $\langle p_T^\parallel \rangle_\Delta$, in other words the uncertainty in $\langle p_T^\parallel \rangle_{p_T^{\text{trk}}, \Delta}$, is shown in table 2 for $R = 0.3$, in events with 0–30% central PbPb collisions. Finally, as shown in table 3, uncertainties in jet reconstruction and track reconstruction in MC events increase together with increasing R , as the UE inside the jet cone gets larger. However, JES difference between quark and gluon jets is smaller for large R parameters, and uncertainties that account for JES differences in data and in MC events therefore decrease.

Although uncertainties in differences in multiplicities are calculated separately, their values are not listed in a table, because they can be approximated from the uncertainties in $\langle p_T^\parallel \rangle$ divided by the average charged particle p_T in that range. In 0–10% central events, for $R = 0.3$, the dominant source is jet reconstruction, with an uncertainty caused by an upward fluctuation in the background under the leading jet, which is followed by the uncertainty in track reconstruction, and residual track reconstruction in data and in MC events that change by 0.5–1.5 particles, as a function of A_J . The uncertainties increase with R and with centrality from peripheral to central collisions.

Δ	$R = 0.2$		$R = 0.4$		$R = 0.5$	
	<0.2	0.2–2.0	<0.2	0.2–2.0	<0.2	0.2–2.0
Jet reconstruction	1	0.1–0.4	1	0.1–0.5	1	0.1–0.7
Data/MC differences for JES	2	0.1–0.5	2	0.1–0.4	2	0.1–0.3
Fragmentation dependent JES	1	0.1–0.4	1	0.1–0.3	1	0.1–0.3
Track corrections	2	0.2–0.7	2	0.1–1.1	2	0.1–1.1
Data/MC differences for tracking	1	0.1–0.2	1	0.1	1	0.1
Total	3	0.2–0.9	3	0.3–1.1	3	0.2–1.1

Table 3. Systematic uncertainties in $\langle p_T^{\parallel} \rangle_{p_T^{\text{trk}}, \Delta}$ in 0–30% PbPb collisions are shown for jets clustered with distance parameters of 0.2, 0.4 and 0.5. Uncertainties are shown as shifts in the values in units of GeV (rather than as fractions) for two Δ selections.

8 Results

8.1 Dependence of the p_T balance in pp and PbPb on opening angles around jets

Angular distribution of the p_T relative to the axis defined by the parton direction is a key for studying QCD processes responsible for parton energy loss. In models, large-angle modifications in the event due to jet quenching have been accommodated qualitatively through a response triggered in the hydrodynamic medium by the deposited energy [47] and through the cascade of gluons created in medium-induced radiation processes [48–51]. Moreover, some MC implementations of jet quenching that modify partonic showers in PYTHIA, such as Q-PYTHIA, can generate soft particles at angles $\Delta > 0.8$, but this treatment modifies the fragmentation functions more severely than found in data [52, 53]. Angular scales for different jet quenching mechanisms in perturbative QCD are related to momentum scales through time evolution of partonic interactions [23]. Especially for QCD cascades in a sufficiently large medium, angular broadening is independent of the path length, and this mechanism might therefore produce a cumulative effect even after taking averages over different events where jets travel different path lengths in the QGP. The medium response may not have the same correlation between angular and momentum scales. The relative importance of each mechanism is unknown. Measuring the p_T spectra of $\langle p_T^{\parallel} \rangle$ as a function of Δ from the jet axis, denoted as $\langle p_T^{\parallel} \rangle_{p_T^{\text{trk}}, \Delta}$, as discussed in section 6, can provide information on the momentum scales at which certain quenching mechanisms become dominant.

The analysis is performed for pp collisions, and two PbPb centrality selections of 30–100% and 0–30%. The resulting differential distributions in $\langle p_T^{\parallel} \rangle_{p_T^{\text{trk}}, \Delta}$ are shown for different regions of track p_T (in terms of the colored boxes) as a function of Δ in the upper row of figure 1. The sum of $\langle p_T^{\parallel} \rangle_{p_T^{\text{trk}}, \Delta}$ for different p_T^{trk} ranges as a function of Δ , $\langle p_T^{\parallel} \rangle_{\Delta}$, are given by the open markers, and follow the leading jet at small Δ and subleading jet at large Δ . The cumulative values, $\langle p_T^{\parallel} \rangle_{[0, \Delta]}$ (i.e. from summing and smoothing the $\langle p_T^{\parallel} \rangle_{\Delta}$ over bins in Δ , starting at $\Delta = 0$ and ending at the point of interest) are shown as dashed lines for pp and solid lines for PbPb. These lines demonstrate the evolution of

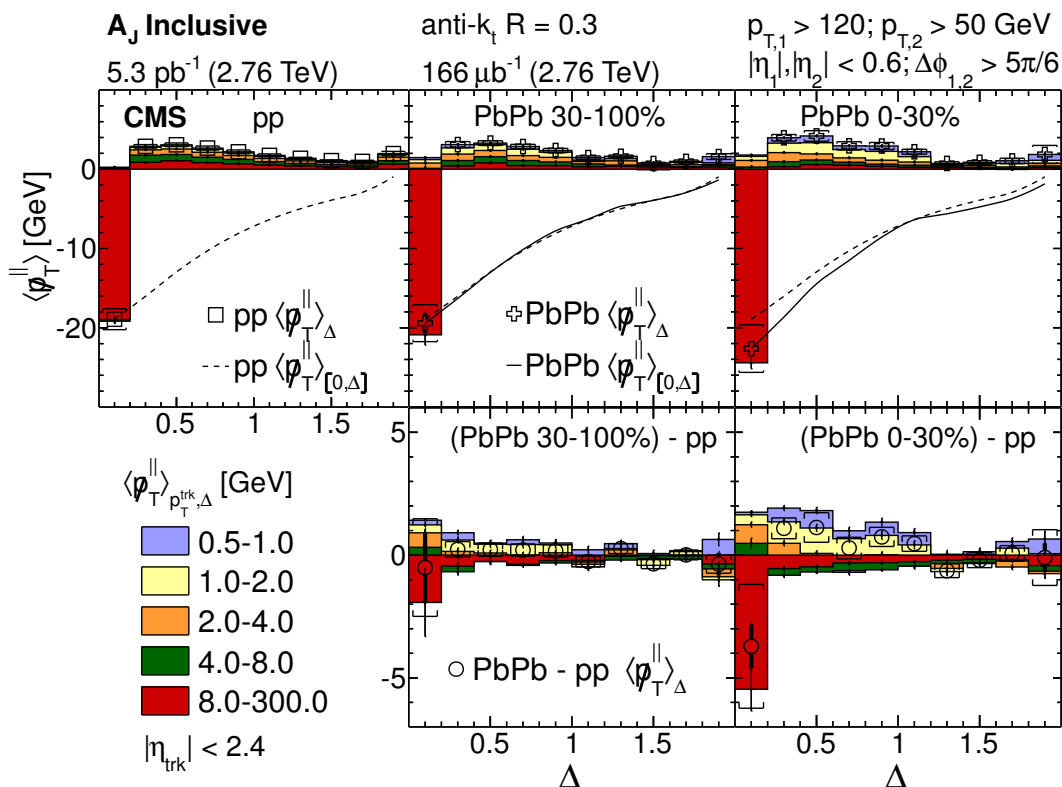


Figure 1. Upper row: $\langle p_T^{\parallel} \rangle_{p_T^{\text{trk}}, \Delta}$ distributions for pp, and for 30–100% and 0–30% PbPb data for five track- p_T ranges (colored boxes), for momentum ranges from $0.5 < p_T < 1$ GeV (light blue) to $8 < p_T < 300$ GeV (red), as a function of Δ . Also shown is $\langle p_T^{\parallel} \rangle_{\Delta}$ as a function of Δ for pp (open squares) and PbPb data (open plus symbols). Dashed lines (pp) and solid lines (PbPb) show $\langle p_T^{\parallel} \rangle_{[0,\Delta]}$ (i.e. integrating the $\langle p_T^{\parallel} \rangle_{\Delta}$ over Δ from $\Delta = 0$ up to the point of interest). Lower row: difference between the PbPb and pp $\langle p_T^{\parallel} \rangle_{p_T^{\text{trk}}, \Delta}$ distributions according to the range in p_T , as a function of Δ (colored boxes), and difference of $\langle p_T^{\parallel} \rangle_{\Delta}$ as a function of Δ (open circles), error bars and brackets represent statistical and systematic uncertainties, respectively.

the overall p_T balance from small to large distances relative to the jet axis, reaching an overall balance close to zero only at large radii. The cumulative curve in PbPb collisions for 0–30% centrality is slightly narrower than for pp collisions.

The distributions in pp collisions have characteristic features, and understanding these is important for interpreting the PbPb results. The magnitude of the $\langle p_T^{\parallel} \rangle_{\Delta}$ in the first bin, with $\Delta < 0.2$, is related to the average dijet imbalance, and takes a negative value indicating that the momentum projection points along the direction of the leading jet. In the rest of the Δ bins, $\langle p_T^{\parallel} \rangle_{\Delta}$ takes a positive value, and $\langle p_T^{\parallel} \rangle_{p_T^{\text{trk}}, \Delta}$ for lower track p_T make up larger fractions of $\langle p_T^{\parallel} \rangle_{\Delta}$. We refer to the $\langle p_T^{\parallel} \rangle_{p_T^{\text{trk}}, \Delta}$ and $\langle p_T^{\parallel} \rangle_{\Delta}$ for bins with $\Delta > 0.2$ as the “balancing distribution” of the corresponding quantity, because they reduce the large p_T imbalance observed in the first bin in Δ . The balancing distribution has a peak in the range $0.4 < \Delta < 0.6$, which is at the most likely Δ position for a third jet relative to the subleading jet.

In PbPb collisions, the peak of the balancing $\langle p_T^{\parallel} \rangle_{\Delta}$ distribution shifts towards smaller angles ($0.2 < \Delta < 0.4$). This can be due to the modification in the fragmentation of the

leading and subleading jets after quenching, as it occurs at angles close to their axes, where the low- p_T particles make largest contributions. It is therefore not possible to claim a direct relation between the peak position of the balancing $\langle \cancel{p}_T^\parallel \rangle_\Delta$ distribution and the location of other jets in the event, unless only the highest- p_T particles are considered, i.e. not likely to be related to the leading and subleading jets at large Δ values. The peak position of the balancing $\langle \cancel{p}_T^\parallel \rangle_{p_T^{\text{trk}}, \Delta}$ distribution of the highest- p_T particles is located at the same place as in pp collisions ($0.4 < \Delta < 0.6$), but with smaller magnitude. This suggests that the position of a third jet relative to the subleading jet is not modified significantly. However, the magnitude of $\langle \cancel{p}_T^\parallel \rangle_{p_T^{\text{trk}}, \Delta}$ for tracks with $8 < p_T < 300$ GeV associated with the third jet can be reduced for several reasons, such as quenching of the third jet, which makes its fragmentation softer, or a change in the ordering of the jets relative to original partonic conditions, i.e. leading parton losing more energy compared to the subleading parton, which causes the third jet to be found in the leading jet hemisphere, instead of the subleading jet hemisphere.

A comparison of pp and PbPb collisions is provided in the lower row of figure 1, showing the difference in PbPb and pp for $\langle \cancel{p}_T^\parallel \rangle_{p_T^{\text{trk}}, \Delta}$, and $\langle \cancel{p}_T^\parallel \rangle_\Delta$ as a function of Δ . For central events, the first bin with $\Delta < 0.2$ $\langle \cancel{p}_T^\parallel \rangle_{p_T^{\text{trk}}, \Delta}$ for high- p_T tracks and $\langle \cancel{p}_T^\parallel \rangle_\Delta$ point in the leading jet direction, although the excess is not significant. While in the second bin with $0.2 < \Delta < 0.4$, there is a significant positive excess in $\langle \cancel{p}_T^\parallel \rangle_\Delta$. The excess towards the subleading jet in this bin may either be because the leading jet is narrower, or the subleading jet wider in PbPb collisions compared to pp collisions. The excess in $\langle \cancel{p}_T^\parallel \rangle_\Delta$ along the subleading jet direction extends up to larger angles ($\Delta \approx 1-1.2$), with decreasing significance. In this angular range, there is an excess in $\langle \cancel{p}_T^\parallel \rangle_{p_T^{\text{trk}}, \Delta}$ for tracks with p_T that fall in the ranges of 0–0.5, 0.5–1, and 1–2 GeV, and a depletion for particles with $p_T > 4$ GeV. This is consistent with results shown in the previous section and earlier CMS studies that demonstrate that the small-angle imbalance towards the leading jet is compensated by particles of small p_T emitted at large angles to the jet axes [12].

8.2 Study of the p_T balance in pp and PbPb collisions, as a function of opening angles around jets in bins of A_J

More information can be obtained by repeating the previous study as a function of dijet asymmetry A_J . The results for a sample containing more balanced dijets ($A_J < 0.22$) is shown in figure 2, again comparing pp data with two PbPb centrality bins. As expected, $\langle \cancel{p}_T^\parallel \rangle_\Delta$ and $\langle \cancel{p}_T^\parallel \rangle_{p_T^{\text{trk}}, \Delta}$ for all track p_T take smaller values compared to inclusive A_J selection, meaning that events with a more balanced dijet selection show an overall better p_T balance in both small $\Delta < 0.2$, as well as larger Δ . This is also seen in the difference in $\langle \cancel{p}_T^\parallel \rangle_\Delta$ for PbPb and pp collisions, although, as before, an preference of $\langle \cancel{p}_T^\parallel \rangle_{p_T^{\text{trk}}, \Delta}$ for low- p_T tracks to point along the subleading side can be seen for central PbPb events.

Complementary to the selection of more balanced dijets, figure 3 shows a selection for unbalanced dijets with $A_J > 0.22$. The A_J selection is reflected in the overall larger contributions in the small- and large-angle regions relative to the jet axes. This large A_J selection, which enhances the fraction of jets having undergone significant energy loss in PbPb collisions, also enhances the differences between PbPb and pp, as shown in the lower row of figure 3.

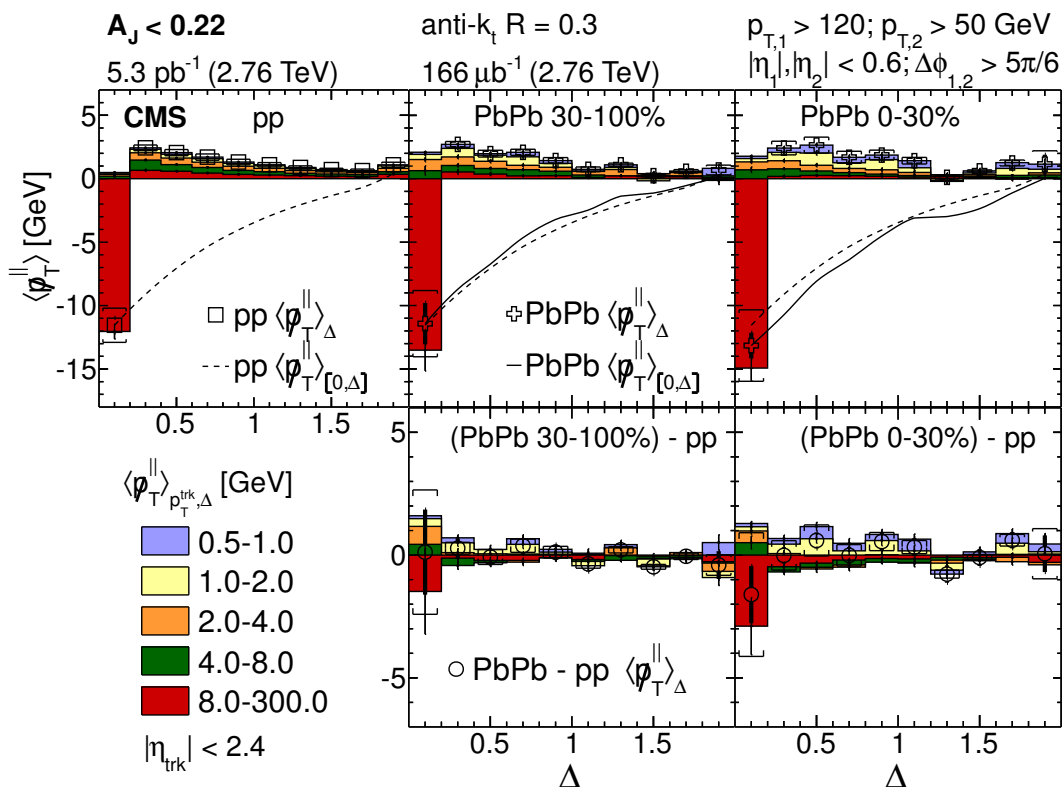


Figure 2. Same as figure 1, but with a balanced dijet selection ($A_J < 0.22$). Upper row: $\langle p_T^{\parallel} \rangle_{p_T^{\text{trk}}, \Delta}$ distributions for pp, and for 30–100% and 0–30% PbPb data for five track p_T ranges (colored boxes), as a function of Δ . Also shown is $\langle p_T^{\parallel} \rangle_{\Delta}$ as a function of Δ for pp (open squares) and for PbPb data (open plus symbols). Dashed lines (pp) and solid lines (PbPb) show $\langle p_T^{\parallel} \rangle_{[0, \Delta]}$ (i.e. integrating the $\langle p_T^{\parallel} \rangle_{\Delta}$ over Δ from $\Delta = 0$ up to the point of interest). Lower row: difference in the $\langle p_T^{\parallel} \rangle_{p_T^{\text{trk}}, \Delta}$ distributions for the PbPb and pp according to the range in p_T , as a function of Δ (colored boxes), and difference of $\langle p_T^{\parallel} \rangle_{\Delta}$ as a function of Δ (open circles). Error bars and brackets represent statistical and systematic uncertainties, respectively. The y-axis range on the top panels are smaller than in figure 1.

It is important to note that in pp collisions, only 30% of selected dijet events have $A_J > 0.22$, but this number increases to 42% for central PbPb selections. This again suggests the presence of an additional mechanism creating asymmetric dijets in PbPb, i.e. parton energy loss in the medium. Consistent with this picture, the A_J dependence of the $\langle p_T^{\parallel} \rangle_{p_T^{\text{trk}}, \Delta}$ distributions in PbPb and pp collisions and their difference suggests that asymmetric dijet systems in pp and PbPb collisions are created through different mechanisms, with semi-hard radiation (e.g., three-jet events) dominating pp collisions. In contrast, a large fraction of asymmetric dijet events in PbPb is created through a differential energy loss mechanism as the partons traverse the medium, which leads to the observed excess in $\langle p_T^{\parallel} \rangle_{p_T^{\text{trk}}, \Delta}$ for the low- p_T bins. The depletion of high- p_T particle contributions at large angles in PbPb is more dominant with $A_J > 0.22$ relative to an inclusive A_J selection, because of the difference in relative fractions of three-jet events among all selected events.

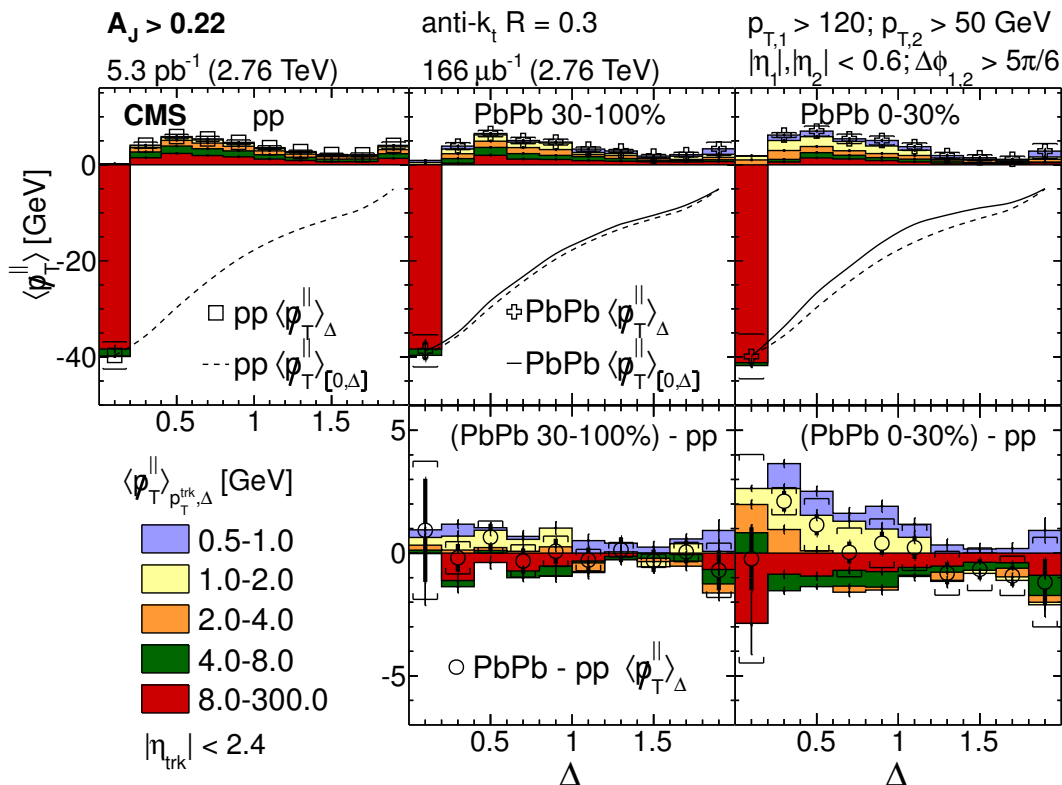


Figure 3. Same as figure 1, but with an unbalanced dijet selection ($A_J > 0.22$). Upper row: $\langle p_T^{\parallel} \rangle_{p_T^{\text{trk}}, \Delta}$ distributions for pp, and for 30–100% and 0–30% PbPb data for five track p_T ranges, as a function of Δ . Also shown is $\langle p_T^{\parallel} \rangle_{\Delta}$ as a function of Δ for pp and for PbPb data. Dashed lines (pp) and solid lines (PbPb) show $\langle p_T^{\parallel} \rangle_{[0, \Delta]}$ (i.e. integrating the $\langle p_T^{\parallel} \rangle_{\Delta}$ over Δ from $\Delta = 0$ up to the point of interest). Lower row: difference in the $\langle p_T^{\parallel} \rangle_{p_T^{\text{trk}}, \Delta}$ distributions for the PbPb and pp. Error bars and brackets represent statistical and systematic uncertainties, respectively. The y -axis range on the top panels are larger than in figure 1.

8.3 Dependence of dijet asymmetry on p_T balance and multiplicity difference in jet hemispheres

To study the p_T flow relative to the dijet system as a function of event properties, such as centrality and A_J , in more detail, the $\langle p_T^{\parallel} \rangle_{p_T^{\text{trk}}, \Delta}$ is summed over all annuli to obtain $\langle p_T^{\parallel} \rangle_{p_T^{\text{trk}}}$, i.e. the average p_T balance in the event calculated for a given range of track p_T . In figure 4, we display $\langle p_T^{\parallel} \rangle_{p_T^{\text{trk}}}$ for different ranges of track p_T (displayed in terms of the colored boxes) as a function of A_J , ranging from almost balanced to very unbalanced dijets in pp collisions, and in four selections of PbPb centrality from most peripheral to most central. The balance in the event for all tracks with $p_T > 0.5$ GeV, denoted as $\langle p_T^{\parallel} \rangle_{\Sigma}$, which is obtained by adding up the $\langle p_T^{\parallel} \rangle_{p_T^{\text{trk}}}$ for different p_T ranges, is also included, and shown as open markers, with associated systematic uncertainties as brackets around the points. In PbPb events, overall p_T is balanced to better than 10 GeV, i.e. $|\langle p_T^{\parallel} \rangle_{\Sigma}| < 10$ GeV for all A_J selections. The small negative trend in $\langle p_T^{\parallel} \rangle_{\Sigma}$ as a function of A_J is observed also in pp events, and in generator-level PYTHIA events, once the p_T threshold set on charged particles and the acceptance of the tracker are imposed.

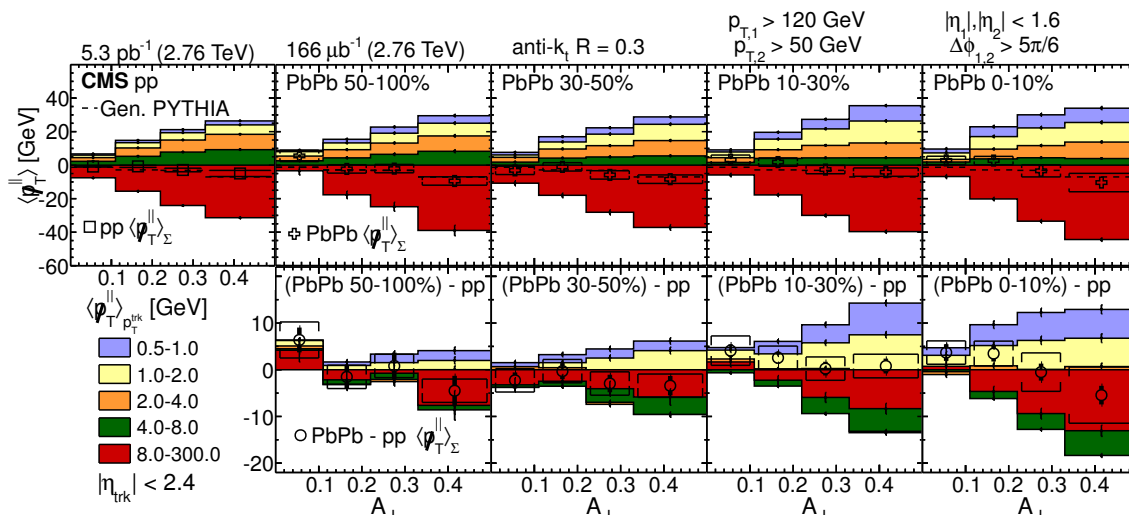


Figure 4. Upper row has $\langle p_T^\parallel \rangle_{p_T^{\text{trk}}}$ and $\langle p_T^\parallel \rangle_\Sigma$ in pp collisions (leftmost) and in four selections of PbPb for collision centralities from 50–100% to 0–10%. The open markers show $\langle p_T^\parallel \rangle_\Sigma$, p_T balance for tracks with $0.5 < p_T < 300$ GeV, while the colored boxes show the $\langle p_T^\parallel \rangle_{p_T^{\text{trk}}}$ contributions for different track p_T ranges. For each panel, $\langle p_T^\parallel \rangle_{p_T^{\text{trk}}}$ and $\langle p_T^\parallel \rangle_\Sigma$ values are shown as a function of dijet asymmetry. The lower row shows the difference between $\langle p_T^\parallel \rangle_{p_T^{\text{trk}}}$ and $\langle p_T^\parallel \rangle_\Sigma$ for PbPb and pp data. Error bars and brackets represent statistical and systematic uncertainties, respectively.

When selecting events containing dijets with $A_J > 0.11$, an expected excess of high- p_T particles in the direction of the leading jet (indicated by the red areas in figure 4) is seen for all selections in pp and PbPb collisions. For pp and peripheral PbPb collisions, this excess is mostly balanced by particles with intermediate p_T of 2–8 GeV. Going to more central collisions, $\langle p_T^\parallel \rangle_{p_T^{\text{trk}}}$ on the subleading jet side is modified from the intermediate p_T range towards low p_T (0.5–2 GeV). This effect is most pronounced for events with large A_J in central PbPb collisions.

The lower row of figure 4 shows the difference between $\langle p_T^\parallel \rangle_{p_T^{\text{trk}}}$ in PbPb and pp collisions, after requiring the specific PbPb collision centralities and dijet imbalance. While the contributions from different p_T ranges are similar for pp and peripheral PbPb collisions, a difference can be seen for central collisions, where a significant excess of low- p_T charged particles is observed for asymmetric jets in PbPb collisions. Systematic uncertainties are shown only for $\langle p_T^\parallel \rangle_\Sigma$, and not for $\langle p_T^\parallel \rangle_{p_T^{\text{trk}}}$. Uncertainties in $\langle p_T^\parallel \rangle_\Sigma$ provide an upper bound on systematic uncertainties for individual p_T ranges, as uncertainties in low- p_T particles are, in fact, significantly smaller. The excess observed in low- p_T particles in the range of 0.5–2 GeV has therefore a significance of 3–4 standard deviations for $A_J > 0.11$ for most central events. The difference in $\langle p_T^\parallel \rangle$ between PbPb and pp collisions for all tracks with $p_T > 0.5$ GeV is consistent with zero across all centrality and A_J selections.

The overall p_T balance observed through $\langle p_T^\parallel \rangle_\Sigma$ in PbPb events agrees with pp events, within systematic and statistical uncertainties, over all ranges of A_J and centrality, while the $\langle p_T^\parallel \rangle_{p_T^{\text{trk}}}$ distributions show excess of low- p_T particles. This implies that there are more particles in the subleading jet hemispheres compared to the leading jet hemispheres, because more particles are required to obtain the same p_T sum.

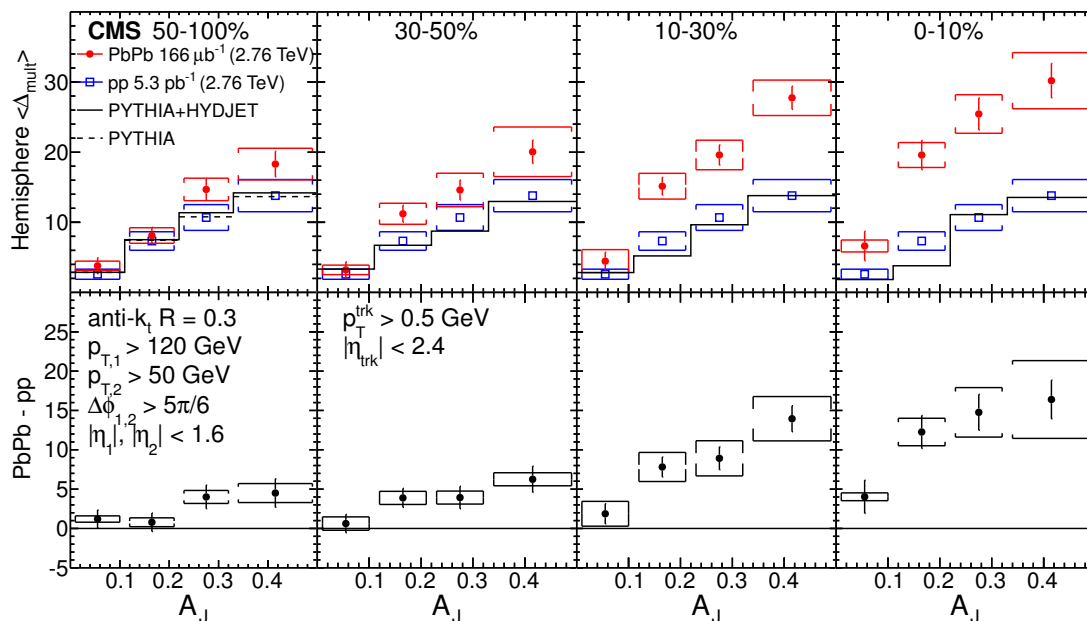


Figure 5. Upper panels show the comparison of the mean difference in multiplicity $\langle \Delta_{\text{mult}} \rangle$ between the subleading jet hemisphere and leading jet hemisphere, as a function of dijet asymmetry A_J for pp (blue squares), PbPb (red filled circles), PYTHIA (dashed histogram), and PYTHIA+HYDJET events (black histogram). The centralities of PbPb collisions are 50–100%, 30–50%, 10–30 %, and 0–10%, respectively, from leftmost to rightmost panel. Lower panels provide the difference in $\langle \Delta_{\text{mult}} \rangle$ between PbPb and pp collisions. Statistical and systematic uncertainties are shown as error bars and brackets, respectively.

Figure 5 shows the mean difference in multiplicities between leading and subleading jet hemispheres, denoted as $\langle \Delta_{\text{mult}} \rangle$, as a function of A_J and collision centrality. The $\langle \Delta_{\text{mult}} \rangle$ is presented for both PbPb and pp collisions. Measurements in pp collisions are in good agreement with PYTHIA and PYTHIA+HYDJET simulations. In general, the $\langle \Delta_{\text{mult}} \rangle$ increases as a function of A_J in pp, PbPb, PYTHIA, and PYTHIA+HYDJET events. The events in pp collisions with large A_J contain a larger fraction of three-jet or multijet events, where more particles are produced in the direction of the subleading jet. The observed increase in $\langle \Delta_{\text{mult}} \rangle$ for pp collisions with increasing A_J is therefore expected. Going from peripheral (50–100%) to central (0–10%) PbPb events, for a given A_J selection an excess in $\langle \Delta_{\text{mult}} \rangle$ is visible compared to pp collisions. The difference in $\langle \Delta_{\text{mult}} \rangle$ between pp and PbPb collisions increases monotonically as a function of A_J at all collision centralities, with the biggest effect seen for most central PbPb collisions. This is consistent with the expected dependence of medium-induced energy loss on collision centrality, where systems of the largest size (i.e. smallest centrality) should show the largest medium-related effects. The multiplicity difference is up to ≈ 15 particles in the most central 0–10 % collisions.

8.4 Dependence of transverse momentum balance on jet distance parameter R

In pp collisions, jets clustered with small R are narrower and fragment into components with higher p_T than jets clustered with large R . In addition, using small R tends to

bias the clustered jets to contain a larger fraction of quark jets [54, 55]. Changing the R parameter can provide a handle on the size and shower profiles of individual jets. In heavy ion collisions, studying the R dependence of momentum flow in dijet events makes it possible to investigate whether jet quenching mechanisms act differently on jets with different fragmentation patterns on a jet-by-jet basis.

It is important to note that there is an overlap in the final set of dijet events obtained for different R parameters, and therefore it is not possible to interpret the dependence of the p_T -balance distributions on R as simply a dependence on jet size. A change in R can induce a modification in \cancel{p}_T^{\parallel} in two ways: events that satisfy the dijet requirements for one R can fail for another R value, or events that satisfy the dijet requirements for both R parameters, but for which the ordering of jets change, can impact ϕ_{dijet} , as well as the value of parameters used in the binning of the measurements, such as A_J and Δ .

The requirements on the p_T of leading and subleading jets are the main sources of variations in the final set of dijet events for different R parameters. For each R , a jet p_T selection translates into a different requirement on initial parton p_T . A smaller fraction of the initial energy of the parton is recovered using jets of smaller size. Although fewer events pass the dijet requirement for $R = 0.2$ jets, strictly speaking, such events do not form a subset of dijet events with larger R parameters. A small fraction of $R = 0.2$ dijet events (4–7% in PbPb collisions and 2–4% in pp collisions) does not satisfy the dijet requirements for other R values, mainly because jets fall outside of the η range or the $\Delta\phi$ requirement for the dijet pair. This can happen because of the merging of the subleading and third jets, and because of the resolution in jet angular direction. Such events make up a statistically negligible contribution to the results and are therefore not the focus of the discussion.

The fraction of events that pass the dijet selection both for the largest $R = 0.5$ and for other values are shown in the second column of table 4, without matching the directions of the jets. Compared to pp collisions, the fraction of events that pass both cutoffs on jets is reduced in PbPb collisions more rapidly as R decreases. This observation is qualitatively consistent with the measurement showing that inclusive jet suppression is smaller in PbPb collisions for large R values [56], which can be interpreted as due to the recovery of part of the energy lost in the initial hard scatter of partons.

Additional information can therefore be extracted by requiring the leading and subleading jets with a given R to be in the same direction as the corresponding jets found using $R = 0.5$. As shown in the third column of table 4, the fraction of such events is similar for pp and PbPb collisions. These events produce almost no change in ϕ_{dijet} and the jet axes, which change only slightly due to jet angular resolution, and therefore yield approximately the same \cancel{p}_T^{\parallel} . However, these events can accommodate the change in the p_T of jets that originate from the same initial hard-scattered parton for different R parameters. For jets matched to each other spatially, the ratio of the p_T of the leading or subleading jet at some given R to respective jets with $R = 0.5$, $\langle p_{T,1(2)}^R / p_{T,1(2)}^{R=0.5} \rangle$, is calculated and the values are shown in columns 4 and 5 in table 4. As expected, in both PbPb and pp collisions, $\langle p_{T,1}^R / p_{T,1}^{R=0.5} \rangle$ and $\langle p_{T,2}^R / p_{T,2}^{R=0.5} \rangle$ are reduced as R gets smaller. In PbPb collisions, a smaller fraction of jet p_T is recovered at small R for both the leading and subleading jets, which may be due to the broadening of quenched jets. This effect is larger for the subleading than for the leading jet.

R	Additional dijet selection [%]	Matched jet directions [%]	$\langle p_{T,1}^R/p_{T,1}^{R=0.5} \rangle$	$\langle p_{T,2}^R/p_{T,2}^{R=0.5} \rangle$	Swapped jet directions [%]
PbPb					
0.2	48 ± 2	83 ± 5	0.89 ± 0.001	0.79 ± 0.002	10 ± 3
0.3	62 ± 2	90 ± 4	0.93 ± 0.002	0.88 ± 0.004	7 ± 3
0.4	77 ± 1	94 ± 3	0.96 ± 0.002	0.94 ± 0.005	3 ± 2
pp					
0.2	58 ± 2	83 ± 5	0.91 ± 0.001	0.83 ± 0.002	14 ± 3
0.3	73 ± 2	90 ± 4	0.95 ± 0.001	0.90 ± 0.001	8 ± 3
0.4	86 ± 1	95 ± 3	0.98 ± 0.001	0.96 ± 0.001	4 ± 2

Table 4. Overlap in event selections for 0–100% PbPb and pp collisions. The second column gives the percentage of events that pass dijet selections and a tight pseudorapidity requirement ($|\eta| < 0.6$) for $R = 0.5$, and an additional dijet selection also required for a smaller R value. In columns 3–6 the leading and subleading jets with $R = 0.5$ are matched to the leading and subleading jets with smaller R values, requiring only $R = 0.5$ selection on jets. The third column shows the percentage of these events where both leading and subleading jets point in the same direction ($\Delta_i = \sqrt{(\eta_i^R - \eta_i^{R=0.5})^2 + (\phi_i^R - \phi_i^{R=0.5})^2} < 0.5$ for $i = 1$ and 2). The average value of the ratio of p_T of the leading and subleading jets at jet for a given R , to their p_T for $R = 0.5$ are shown in the fourth and fifth columns, respectively. The sixth column shows percentage of events in which subleading jets with the given R parameter match the $R = 0.5$ leading jet, and the leading jet matches the $R = 0.5$ subleading jet.

As R parameters become smaller, leading and subleading jets fall below the p_T requirements. Most of the time, the leading jet satisfies the p_T selection for $R = 0.5$, but falls below the threshold for smaller R , because the subleading jet p_T is already biased towards values above the 50 GeV threshold by the leading jet with $p_T > 120$ GeV in the event. However, as shown in figures 2 and 3, for $R = 0.3$ jets the $\langle \cancel{p}_T^\parallel \rangle_{p_T^{\text{trk}}, \Delta}$ signal is dominated by dijet events with large imbalance, which is true for all other R parameters as well. For events with $A_J > 0.22$, $\langle p_{T,2} \rangle \approx 70\text{--}80$ GeV is sufficiently close to the 50 GeV threshold for subleading jets falling below the threshold to create sizable effects on the results.

The last column of table 4 gives the fraction of events with swapped leading and subleading jets compared to those with $R = 0.5$. For these events, the \cancel{p}_T^\parallel has an opposite sign relative to the value for $R = 0.5$, as ϕ_{dijet} points in the opposite hemisphere. Especially in pp collisions, swapping of the leading and subleading jet is the main source of events in which the jet directions are not matched. In PbPb collisions, swapping is slightly less frequent than in pp collisions, suggesting that the third jet may be replacing the subleading jet. For events that satisfy dijet requirements for different R parameters, the \cancel{p}_T^\parallel in each event can still change as a function of R because of the swapping of jets in the dijet pairs, and the replacement of the subleading jet by the third jet.

The dependence of $\langle \cancel{p}_T^\parallel \rangle_{p_T^{\text{trk}}, \Delta}$ on Δ and R is shown in figure 6, without any A_J requirement, for pp and for PbPb events with 0–30% centralities. The R -dependent evolution in pp collisions, which is attributed to the softening and broadening of jets, can be seen

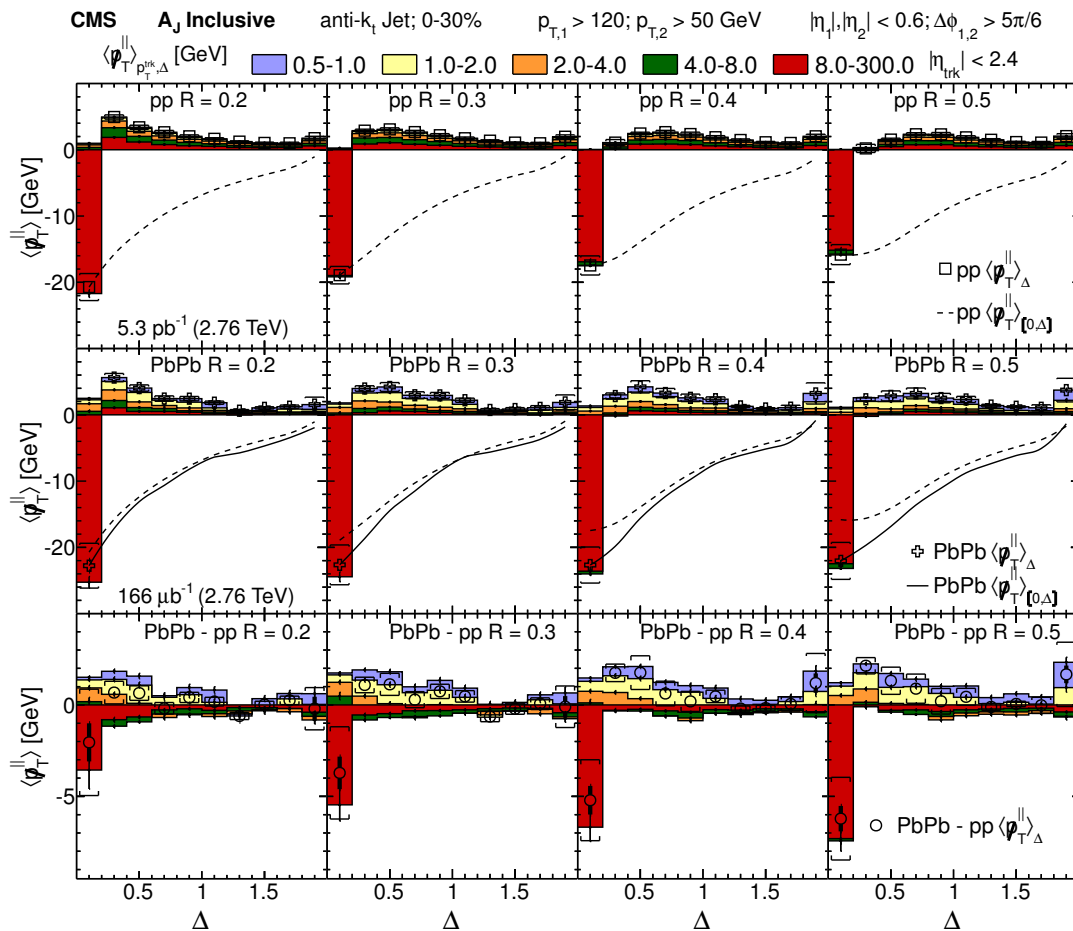


Figure 6. Upper row shows $\langle p_T^{\parallel} \rangle_{p_T^{\text{trk}},\Delta}$ in pp collisions as a function of Δ , for a distance parameter $R = 0.2, 0.3, 0.4$, and 0.5 , from left to right for different ranges of track p_T , and $\langle p_T^{\parallel} \rangle_{\Delta}$ (i.e. $\langle p_T^{\parallel} \rangle_{p_T^{\text{trk}},\Delta}$ summed over all p_T for a given Δ bin). Dashed lines indicate cumulative results for $\langle p_T^{\parallel} \rangle_{[0,\Delta]}$ in pp, for each distance parameter (i.e. integrating $\langle p_T^{\parallel} \rangle_{\Delta}$ over the Δ range from $\Delta = 0$ to the point of interest). Middle row provides $\langle p_T^{\parallel} \rangle_{p_T^{\text{trk}},\Delta}$ and $\langle p_T^{\parallel} \rangle_{\Delta}$ in PbPb collisions of centrality range 0–30% as a function of Δ , for distance parameters $R = 0.2, 0.3, 0.4$, and 0.5 from left to right. Solid line indicates $\langle p_T^{\parallel} \rangle_{[0,\Delta]}$ in PbPb for each distance parameter. Lower row has the difference between PbPb and pp. Error bars and brackets represent statistical and systematic uncertainties, respectively. The results are inclusive in the dijet asymmetry parameter A_J .

as a shift in the position of the sign change of $\langle p_T^{\parallel} \rangle_{p_T^{\text{trk}},\Delta}$ and as a decrease in the total imbalance within the jet cones $\Delta \lesssim 0.2\text{--}0.4$. Moreover, the peaking point of the balancing distribution shifts towards larger Δ , as jet distance parameter R increases (from $\Delta = 0.2\text{--}0.4$ for $R = 0.2$ jets, to $\Delta = 0.6\text{--}1.0$ for $R = 0.5$ jets). As stated for $R = 0.3$ jets in section 8.1, the peak position is correlated with the most likely position of the third jet relative to the subleading jet, which also moves to larger angles by increasing R .

In the PbPb system, the peak also shifts towards greater Δ , but less than in pp collisions due to the additional soft particles at small angles associated to the quenching of the dijet pair and reduction in the number of high- p_T particles associated with the third

jet. In the PbPb–pp bottom panels, this manifests in the depletion of higher ranges at p_T , 4–8 and 8–300 GeV, which shift to greater angular distance with increasing R . There is a modest increase observed in the excess in the p_T ranges of 0.5–1 and 1–2 GeV with increasing R . The overall distribution in the low- p_T excess in PbPb relative to pp does not change significantly with the distance parameter, and especially not at larger angular distance Δ .

There is a hint that the $\langle p_T^{\parallel} \rangle_{[0,\Delta]}$ distribution in central PbPb collisions, shown by the black curves in figure 6, is narrower than in pp collisions, shown by the dashed black curves, meaning that the slope is larger in PbPb relative to pp collisions. This becomes slightly more significant at $R = 0.5$, where bias in gluon or quark jets that have large angular width becomes smaller. This is also reflected in the increase in the magnitude of $\langle p_T^{\parallel} \rangle_{\Delta}$ in the leading jet direction in the first bin, and in the subleading jet direction in the second bin. This modification is dominated by particles with $p_T > 2$ GeV, and may arise from quenching effects, causing leading jets to narrow or subleading jets to widen in central PbPb relative to pp collisions.

To summarize the dependence of differences in p_T balance among different R bins on A_J , and to investigate the observed changes in the associated track p_T spectrum in more central events, our measurement of the dependence of the p_T balance on R and A_J , is shown in figure 7 for pp and 0–10% central PbPb events, respectively, in the top and middle rows. The leftmost panels correspond to a selection of $R = 0.2$ jets, while the rightmost panels correspond to $R = 0.5$. For pp collisions, there is a slight decrease in the magnitude of signal in each p_T range as R increases. This behavior is consistent with the observed reduction in the incone $\langle p_T^{\parallel} \rangle_{p_T^{\text{trk}},\Delta}$ for high- p_T tracks with $\Delta < 0.2$ shown in the top panels of figure 6 as a function of R , which was discussed above, and is also observed in generator-level PYTHIA. This kind of behavior is not observed in central PbPb events.

The bottom row of figure 7 displays the difference between PbPb and pp results. The R parameter is correlated with a small change in the magnitude of the $\langle p_T^{\parallel} \rangle_{p_T^{\text{trk}}}$ excess of low- p_T particles, as jets of larger R give a greater excess. When p_T ranges 0.5–2.0 GeV are combined, the increase in the low- p_T excess becomes more significant. The systematic uncertainties shown in the plot are dominated primarily by the p_T range 8.0–300.0 GeV, and as such cannot be used to characterize the significance of $\langle p_T^{\parallel} \rangle_{p_T^{\text{trk}}}$ in the low track- p_T ranges, nor the slight dependence on the distance parameter in the low- p_T excess. The sum of track p_T ranges $\langle p_T^{\parallel} \rangle_{\Sigma}$ is insensitive to the distance parameter, and the difference between PbPb and pp collisions is consistent with zero for all R values.

Finally, the multiplicity associated with excess of low- p_T particles shown in figures 6 and 7, and the charged-particle spectrum for $\langle \Delta_{\text{mult}} \rangle$ are given in figure 8 for events with 0–30% centrality, without any A_J requirement, for several distance parameters in pp and PbPb collisions, and for their difference.

In pp collisions the fragmentation of leading jets with high p_T provides more high- p_T and fewer low- p_T particles in the hemisphere of the leading jet relative to the subleading-jet hemispheres. As a result, $\langle d\Delta_{\text{mult}}/dp_T \rangle$ has a positive value for charged particles with $p_T < 8$ GeV and a negative value for charged particles with $p_T > 8$ GeV. Also, in PbPb collisions, $\langle d\Delta_{\text{mult}}/dp_T \rangle$ is positive for particles with $p_T < 8$ GeV and becomes negative

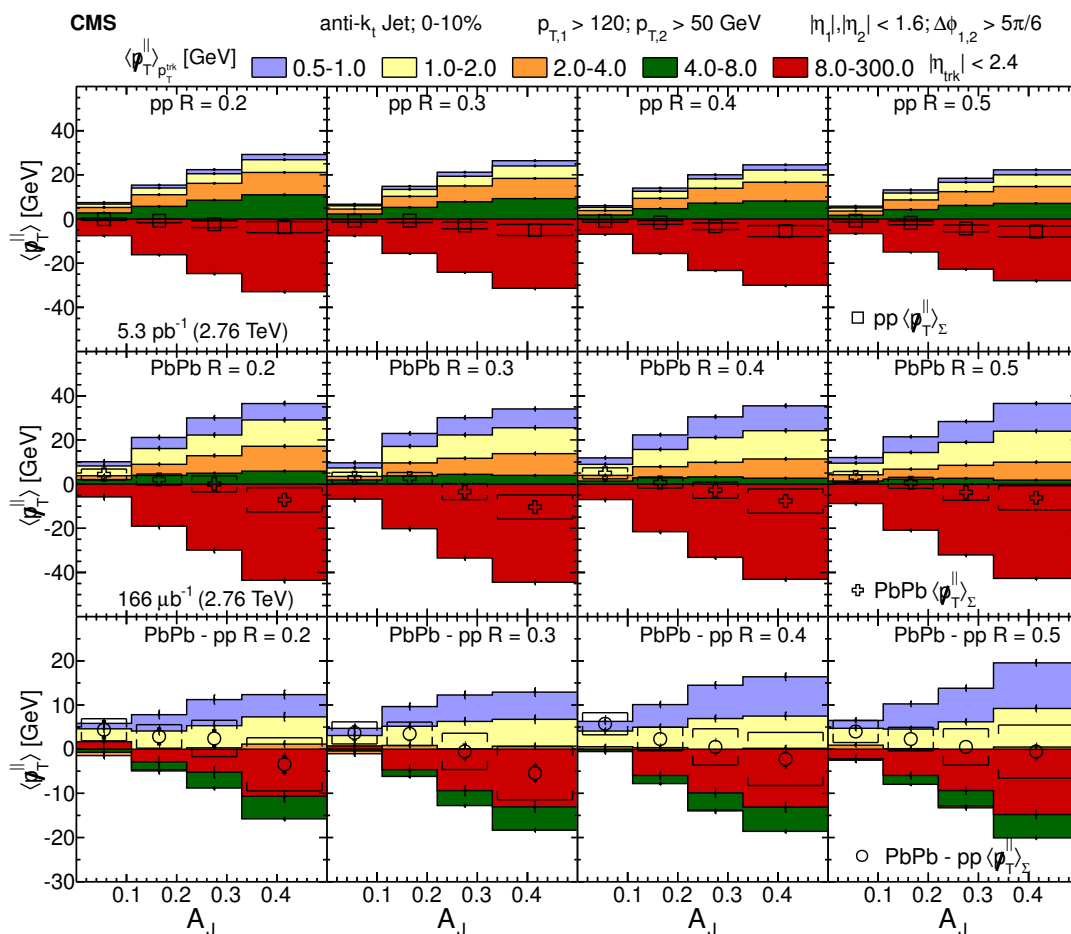


Figure 7. Upper row shows $\langle p_T^\parallel \rangle_{p_T^{\text{trk}}}$ (the individual track p_T) and $\langle p_T^\parallel \rangle_\Sigma$ (sum over all ranges of track p_T) as a function of A_J in pp collisions for distance parameters $R = 0.2, 0.3, 0.4$, and 0.5 , from left to right. The dijet asymmetry ranges from almost balanced ($A_J < 0.11$) to unbalanced ($A_J > 0.33$) dijets. Middle row provides $\langle p_T^\parallel \rangle_{p_T^{\text{trk}}}$ and $\langle p_T^\parallel \rangle_\Sigma$ as a function of A_J in PbPb collisions of centrality range 0–10%, for distance parameter $R = 0.2, 0.3, 0.4$, and 0.5 , from left to right. Lower row has the difference PbPb – pp of the $\langle p_T^\parallel \rangle_{p_T^{\text{trk}}}$, and $\langle p_T^\parallel \rangle_\Sigma$, which are shown in the upper panels. Error bars and brackets represent statistical and systematic uncertainties, respectively.

in the last bin, although the spectrum is much steeper, and has a large excess of soft particles. By taking the difference in $\langle d\Delta_{\text{mult}}/dp_T \rangle$ between PbPb and pp collisions, a significant excess (>5 standard deviations) is observed at $p_T < 2$ GeV, and a depletion at $p_T > 4$ GeV, while there is only a slight excess in the range $2 < p_T < 4$ GeV. Changing R does not have an effect on the results in pp collisions, while in PbPb collisions there is a small enhancement in the excess for low- p_T charged particles as R is increased from 0.2 to 0.5.

9 Summary and conclusions

The transverse momentum flow relative to the dijet axis in PbPb and pp collisions containing jets with large p_T has been studied using data corresponding to integrated luminosities

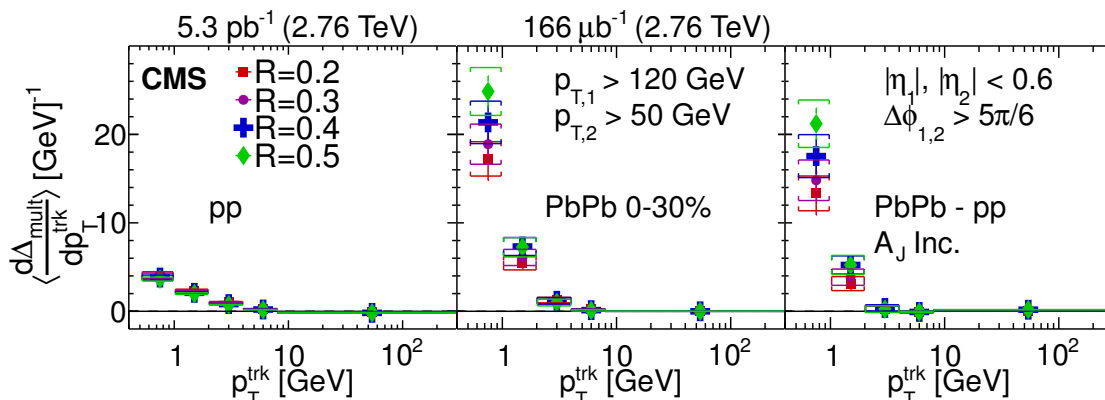


Figure 8. Difference in differential multiplicity $\langle d\Delta_{\text{mult}}/dp_{T^{\text{trk}}} \rangle$ between the away-side and leading-jet hemispheres as a function of track p_T , using an inclusive dijet asymmetry selection. Left panel has measurements in pp for jet radii $R = 0.2, 0.3, 0.4$, and 0.5 , and the middle panel displays similar measurements in PbPb. Right panel provides the difference in $\langle d\Delta_{\text{mult}}/dp_{T^{\text{trk}}} \rangle$ between PbPb and pp collisions for each momentum range. Systematic uncertainties are shown as boxes. Error bars represent statistical uncertainties.

of $166 \mu\text{b}^{-1}$ and 5.3pb^{-1} , respectively, collected at a nucleon-nucleon center-of-mass energy of 2.76 TeV. Dijet events were selected containing a leading jet with transverse momentum $p_{T,1} > 120$ GeV and a subleading jet with $p_{T,2} > 50$ GeV, reconstructed using the anti- k_T algorithm, with distance parameters of $R = 0.2, 0.3, 0.4$ and 0.5 . For PbPb collisions, the dijet events show a larger asymmetry in p_T between the leading and subleading jets than in pp collisions. The multiplicity, angular, and p_T spectra of the radiation balancing this asymmetry are characterized using several techniques as a function of PbPb collision centrality and p_T asymmetry. For a given dijet asymmetry, the imbalance in p_T in PbPb collisions is found to be compensated by particles at $p_T = 0.5\text{--}2$ GeV, whereas in pp collisions most of the momentum balance is found in the p_T range of 2–8 GeV, reflecting a softening of the radiation responsible for the imbalance in p_T of the asymmetric dijet system in PbPb interactions. Correspondingly, a larger multiplicity of associated particles is seen in PbPb than in pp collisions. Both measurements show larger differences between PbPb and pp for more central PbPb collisions. The current data provide the first detailed study of the angular dependence of charged particle contributions to the asymmetry up to large angles from the jet axis ($\Delta = 1.8$). Despite the large shift in the p_T spectrum of particles, the angular pattern of energy flow in PbPb events as a function of Δ matches that seen in pp collisions, especially for small R parameters. The results suggest that either the leading jet is getting narrower, or the subleading jet is getting broader after quenching. In pp collisions, the balancing distribution shifts to larger Δ with increasing distance parameter R , likely because of the presence of a third jet further away from the dijet axis. The shift is more pronounced than in PbPb collisions, where there is an excess of low p_T particles close to the jet axes. These results constrain the redistribution of transverse momentum in the modelling of QCD energy loss processes of partons traversing the hot and dense medium created in heavy-ion collisions.

Acknowledgments

We congratulate our colleagues in the CERN accelerator departments for the excellent performance of the LHC and thank the technical and administrative staffs at CERN and at other CMS institutes for their contributions to the success of the CMS effort. In addition, we gratefully acknowledge the computing centres and personnel of the Worldwide LHC Computing Grid for delivering so effectively the computing infrastructure essential to our analyses. Finally, we acknowledge the enduring support for the construction and operation of the LHC and the CMS detector provided by the following funding agencies: BMFWF and FWF (Austria); FNRS and FWO (Belgium); CNPq, CAPES, FAPERJ, and FAPESP (Brazil); MES (Bulgaria); CERN; CAS, MoST, and NSFC (China); COLCIENCIAS (Colombia); MSES and CSF (Croatia); RPF (Cyprus); MoER, ERC IUT and ERDF (Estonia); Academy of Finland, MEC, and HIP (Finland); CEA and CNRS/IN2P3 (France); BMBF, DFG, and HGF (Germany); GSRT (Greece); OTKA and NIH (Hungary); DAE and DST (India); IPM (Iran); SFI (Ireland); INFN (Italy); MSIP and NRF (Republic of Korea); LAS (Lithuania); MOE and UM (Malaysia); CINVESTAV, CONACYT, SEP, and UASLP-FAI (Mexico); MBIE (New Zealand); PAEC (Pakistan); MSHE and NSC (Poland); FCT (Portugal); JINR (Dubna); MON, RosAtom, RAS and RFBR (Russia); MESTD (Serbia); SEIDI and CPAN (Spain); Swiss Funding Agencies (Switzerland); MST (Taipei); ThEPCenter, IPST, STAR and NSTDA (Thailand); TUBITAK and TAEK (Turkey); NASU and SFFR (Ukraine); STFC (United Kingdom); DOE and NSF (U.S.A.).

We congratulate our colleagues in the CERN accelerator departments for the excellent performance of the LHC and thank the technical and administrative staffs at CERN and at other CMS institutes for their contributions to the success of the CMS effort. In addition, we gratefully acknowledge the computing centres and personnel of the Worldwide LHC Computing Grid for delivering so effectively the computing infrastructure essential to our analyses. Finally, we acknowledge the enduring support for the construction and operation of the LHC and the CMS detector provided by the following funding agencies: the Austrian Federal Ministry of Science, Research and Economy and the Austrian Science Fund; the Belgian Fonds de la Recherche Scientifique, and Fonds voor Wetenschappelijk Onderzoek; the Brazilian Funding Agencies (CNPq, CAPES, FAPERJ, and FAPESP); the Bulgarian Ministry of Education and Science; CERN; the Chinese Academy of Sciences, Ministry of Science and Technology, and National Natural Science Foundation of China; the Colombian Funding Agency (COLCIENCIAS); the Croatian Ministry of Science, Education and Sport, and the Croatian Science Foundation; the Research Promotion Foundation, Cyprus; the Ministry of Education and Research, Estonian Research Council via IUT23-4 and IUT23-6 and European Regional Development Fund, Estonia; the Academy of Finland, Finnish Ministry of Education and Culture, and Helsinki Institute of Physics; the Institut National de Physique Nucléaire et de Physique des Particules / CNRS, and Commissariat à l'Énergie Atomique et aux Énergies Alternatives / CEA, France; the Bundesministerium für Bildung und Forschung, Deutsche Forschungsgemeinschaft, and Helmholtz-Gemeinschaft Deutscher Forschungszentren, Germany; the General Secretariat for Research and Technology, Greece; the National Scientific Research Foundation, and National Innovation Office,

Hungary; the Department of Atomic Energy and the Department of Science and Technology, India; the Institute for Studies in Theoretical Physics and Mathematics, Iran; the Science Foundation, Ireland; the Istituto Nazionale di Fisica Nucleare, Italy; the Ministry of Science, ICT and Future Planning, and National Research Foundation (NRF), Republic of Korea; the Lithuanian Academy of Sciences; the Ministry of Education, and University of Malaya (Malaysia); the Mexican Funding Agencies (CINVESTAV, CONACYT, SEP, and UASLP-FAI); the Ministry of Business, Innovation and Employment, New Zealand; the Pakistan Atomic Energy Commission; the Ministry of Science and Higher Education and the National Science Centre, Poland; the Fundação para a Ciência e a Tecnologia, Portugal; JINR, Dubna; the Ministry of Education and Science of the Russian Federation, the Federal Agency of Atomic Energy of the Russian Federation, Russian Academy of Sciences, and the Russian Foundation for Basic Research; the Ministry of Education, Science and Technological Development of Serbia; the Secretaría de Estado de Investigación, Desarrollo e Innovación and Programa Consolider-Ingenio 2010, Spain; the Swiss Funding Agencies (ETH Board, ETH Zurich, PSI, SNF, UniZH, Canton Zurich, and SER); the Ministry of Science and Technology, Taipei; the Thailand Center of Excellence in Physics, the Institute for the Promotion of Teaching Science and Technology of Thailand, Special Task Force for Activating Research and the National Science and Technology Development Agency of Thailand; the Scientific and Technical Research Council of Turkey, and Turkish Atomic Energy Authority; the National Academy of Sciences of Ukraine, and State Fund for Fundamental Researches, Ukraine; the Science and Technology Facilities Council, U.K.; the US Department of Energy, and the US National Science Foundation.

Individuals have received support from the Marie-Curie programme and the European Research Council and EPLANET (European Union); the Leventis Foundation; the A. P. Sloan Foundation; the Alexander von Humboldt Foundation; the Belgian Federal Science Policy Office; the Fonds pour la Formation à la Recherche dans l'Industrie et dans l'Agriculture (FRIA-Belgium); the Agentschap voor Innovatie door Wetenschap en Technologie (IWT-Belgium); the Ministry of Education, Youth and Sports (MEYS) of the Czech Republic; the Council of Science and Industrial Research, India; the HOMING PLUS programme of the Foundation for Polish Science, cofinanced from European Union, Regional Development Fund; the OPUS programme of the National Science Center (Poland); the Compagnia di San Paolo (Torino); the Consorzio per la Fisica (Trieste); MIUR project 20108T4XTM (Italy); the Thalís and Aristeia programmes cofinanced by EU-ESF and the Greek NSRF; the National Priorities Research Program by Qatar National Research Fund; the Rachadapisek Sompot Fund for Postdoctoral Fellowship, Chulalongkorn University (Thailand); and the Welch Foundation, contract C-1845.

Open Access. This article is distributed under the terms of the Creative Commons Attribution License ([CC-BY 4.0](https://creativecommons.org/licenses/by/4.0/)), which permits any use, distribution and reproduction in any medium, provided the original author(s) and source are credited.

References

- [1] J.D. Bjorken, *Energy loss of energetic partons in QGP: possible extinction of high p_T jets in hadron-hadron collisions*, [FERMILAB-PUB-82-059-THY](https://arxiv.org/abs/hep-th/8205024) (1982).

- [2] PHENIX collaboration, K. Adcox et al., *Suppression of hadrons with large transverse momentum in central Au+Au collisions at $\sqrt{s_{NN}} = 130$ GeV*, *Phys. Rev. Lett.* **88** (2002) 022301 [[nucl-ex/0109003](#)] [[INSPIRE](#)].
- [3] PHENIX collaboration, K. Adcox et al., *Formation of dense partonic matter in relativistic nucleus-nucleus collisions at RHIC: experimental evaluation by the PHENIX collaboration*, *Nucl. Phys. A* **757** (2005) 184 [[nucl-ex/0410003](#)] [[INSPIRE](#)].
- [4] BRAHMS collaboration, I. Arsene et al., *Quark gluon plasma and color glass condensate at RHIC? The perspective from the BRAHMS experiment*, *Nucl. Phys. A* **757** (2005) 1 [[nucl-ex/0410020](#)] [[INSPIRE](#)].
- [5] B.B. Back et al., *The PHOBOS perspective on discoveries at RHIC*, *Nucl. Phys. A* **757** (2005) 28 [[nucl-ex/0410022](#)] [[INSPIRE](#)].
- [6] STAR collaboration, J. Adams et al., *Experimental and theoretical challenges in the search for the quark gluon plasma: the STAR collaboration's critical assessment of the evidence from RHIC collisions*, *Nucl. Phys. A* **757** (2005) 102 [[nucl-ex/0501009](#)] [[INSPIRE](#)].
- [7] ALICE collaboration, *Suppression of charged particle production at large transverse momentum in central Pb-Pb collisions at $\sqrt{s_{NN}} = 2.76$ TeV*, *Phys. Lett. B* **696** (2011) 30 [[arXiv:1012.1004](#)] [[INSPIRE](#)].
- [8] CMS collaboration, *Study of high- p_T charged particle suppression in PbPb compared to pp collisions at $\sqrt{s_{NN}} = 2.76$ TeV*, *Eur. Phys. J. C* **72** (2012) 1945 [[arXiv:1202.2554](#)] [[INSPIRE](#)].
- [9] ATLAS collaboration, *Measurement of charged-particle spectra in Pb+Pb collisions at $\sqrt{s_{NN}} = 2.76$ TeV with the ATLAS detector at the LHC*, *JHEP* **09** (2015) 050 [[arXiv:1504.04337](#)] [[INSPIRE](#)].
- [10] STAR collaboration, C. Adler et al., *Disappearance of back-to-back high p_T hadron correlations in central Au+Au collisions at $\sqrt{s_{NN}} = 200$ GeV*, *Phys. Rev. Lett.* **90** (2003) 082302 [[nucl-ex/0210033](#)] [[INSPIRE](#)].
- [11] ATLAS collaboration, *Observation of a centrality-dependent dijet asymmetry in lead-lead collisions at $\sqrt{s_{NN}} = 2.77$ TeV with the ATLAS detector at the LHC*, *Phys. Rev. Lett.* **105** (2010) 252303 [[arXiv:1011.6182](#)] [[INSPIRE](#)].
- [12] CMS collaboration, *Observation and studies of jet quenching in PbPb collisions at nucleon-nucleon center-of-mass energy = 2.76 TeV*, *Phys. Rev. C* **84** (2011) 024906 [[arXiv:1102.1957](#)] [[INSPIRE](#)].
- [13] CMS collaboration, *Jet momentum dependence of jet quenching in PbPb collisions at $\sqrt{s_{NN}} = 2.76$ TeV*, *Phys. Lett. B* **712** (2012) 176 [[arXiv:1202.5022](#)] [[INSPIRE](#)].
- [14] CMS collaboration, *Studies of dijet transverse momentum balance and pseudorapidity distributions in pPb collisions at $\sqrt{s_{NN}} = 5.02$ TeV*, *Eur. Phys. J. C* **74** (2014) 2951 [[arXiv:1401.4433](#)] [[INSPIRE](#)].
- [15] Y. He, I. Vitev and B.-W. Zhang, *$\mathcal{O}(\alpha_s^3)$ analysis of inclusive jet and di-jet production in heavy ion reactions at the Large Hadron Collider*, *Phys. Lett. B* **713** (2012) 224 [[arXiv:1105.2566](#)] [[INSPIRE](#)].
- [16] C. Young, B. Schenke, S. Jeon and C. Gale, *Dijet asymmetry at the energies available at the CERN Large Hadron Collider*, *Phys. Rev. C* **84** (2011) 024907 [[arXiv:1103.5769](#)] [[INSPIRE](#)].

- [17] G.-Y. Qin and B. Müller, *Explanation of di-jet asymmetry in Pb+Pb collisions at the Large Hadron Collider*, *Phys. Rev. Lett.* **106** (2011) 162302 [Erratum *ibid.* **108** (2012) 189904] [[arXiv:1012.5280](#)] [[INSPIRE](#)].
- [18] J. Casalderrey-Solana, D.C. Gulhan, J.G. Milhano, D. Pablos and K. Rajagopal, *A hybrid strong/weak coupling approach to jet quenching*, *JHEP* **10** (2014) 19 [Erratum *ibid.* **09** (2015) 175] [[arXiv:1405.3864](#)] [[INSPIRE](#)].
- [19] Y. Mehtar-Tani, J.G. Milhano and K. Tywoniuk, *Jet physics in heavy-ion collisions*, *Int. J. Mod. Phys. A* **28** (2013) 1340013 [[arXiv:1302.2579](#)] [[INSPIRE](#)].
- [20] J. Casalderrey-Solana, J.G. Milhano and U.A. Wiedemann, *Jet quenching via jet collimation*, *J. Phys. G* **38** (2011) 035006 [[arXiv:1012.0745](#)] [[INSPIRE](#)].
- [21] CMS collaboration, *Studies of jet quenching using isolated-photon+jet correlations in PbPb and pp collisions at $\sqrt{s_{NN}} = 2.76$ TeV*, *Phys. Lett. B* **718** (2013) 773 [[arXiv:1205.0206](#)] [[INSPIRE](#)].
- [22] CMS collaboration, *Measurement of isolated photon production in pp and PbPb collisions at $\sqrt{s_{NN}} = 2.76$ TeV*, *Phys. Lett. B* **710** (2012) 256 [[arXiv:1201.3093](#)] [[INSPIRE](#)].
- [23] A. Kurkela and U.A. Wiedemann, *Picturing perturbative parton cascades in QCD matter*, *Phys. Lett. B* **740** (2015) 172 [[arXiv:1407.0293](#)] [[INSPIRE](#)].
- [24] CMS collaboration, *Measurement of jet fragmentation into charged particles in pp and PbPb collisions at $\sqrt{s_{NN}} = 2.76$ TeV*, *JHEP* **10** (2012) 087 [[arXiv:1205.5872](#)] [[INSPIRE](#)].
- [25] CMS collaboration, *Modification of jet shapes in PbPb collisions at $\sqrt{s_{NN}} = 2.76$ TeV*, *Phys. Lett. B* **730** (2014) 243 [[arXiv:1310.0878](#)] [[INSPIRE](#)].
- [26] CMS collaboration, *Measurement of jet fragmentation in PbPb and pp collisions at $\sqrt{s_{NN}} = 2.76$ TeV*, *Phys. Rev. C* **90** (2014) 024908 [[arXiv:1406.0932](#)] [[INSPIRE](#)].
- [27] ATLAS collaboration, *Measurement of inclusive jet charged-particle fragmentation functions in Pb+Pb collisions at $\sqrt{s_{NN}} = 2.76$ TeV with the ATLAS detector*, *Phys. Lett. B* **739** (2014) 320 [[arXiv:1406.2979](#)] [[INSPIRE](#)].
- [28] CMS collaboration, *Dependence on pseudorapidity and centrality of charged hadron production in PbPb collisions at a nucleon-nucleon centre-of-mass energy of 2.76 TeV*, *JHEP* **08** (2011) 141 [[arXiv:1107.4800](#)] [[INSPIRE](#)].
- [29] CMS collaboration, *Measurement of the pseudorapidity and centrality dependence of the transverse energy density in PbPb collisions at $\sqrt{s_{NN}} = 2.76$ TeV*, *Phys. Rev. Lett.* **109** (2012) 152303 [[arXiv:1205.2488](#)] [[INSPIRE](#)].
- [30] M. Cacciari, G.P. Salam and G. Soyez, *FastJet user manual*, *Eur. Phys. J. C* **72** (2012) 1896 [[arXiv:1111.6097](#)] [[INSPIRE](#)].
- [31] M. Cacciari, G.P. Salam and G. Soyez, *The anti- k_t jet clustering algorithm*, *JHEP* **04** (2008) 063 [[arXiv:0802.1189](#)] [[INSPIRE](#)].
- [32] CMS collaboration, *The CMS experiment at the CERN LHC*, 2008 *JINST* **3** S08004 [[INSPIRE](#)].
- [33] CMS collaboration, *Description and performance of track and primary-vertex reconstruction with the CMS tracker*, 2014 *JINST* **9** P10009 [[arXiv:1405.6569](#)] [[INSPIRE](#)].
- [34] CMS collaboration, *ECAL 2010 performance results*, CMS-DP-2011-008 (2011).

- [35] CMS collaboration, *Performance of photon reconstruction and identification with the CMS detector in proton-proton collisions at $\sqrt{s} = 8$ TeV*, 2015 *JINST* **10** P08010 [[arXiv:1502.02702](#)] [[INSPIRE](#)].
- [36] CMS collaboration, *Performance of electron reconstruction and selection with the CMS detector in proton-proton collisions at $\sqrt{s} = 8$ TeV*, 2015 *JINST* **10** P06005 [[arXiv:1502.02701](#)] [[INSPIRE](#)].
- [37] CMS collaboration, *Electromagnetic calorimeter calibration with 7 TeV data*, CMS-PAS-EGM-10-003 (2010).
- [38] CMS collaboration, *Performance of the CMS hadron calorimeter with cosmic ray muons and LHC Beam Data*, 2010 *JINST* **5** T03012 [[arXiv:0911.4991](#)] [[INSPIRE](#)].
- [39] USCMS, ECAL/HCAL collaboration, S. Abdullin et al., *The CMS barrel calorimeter response to particle beams from 2 GeV/c to 350 GeV/c*, *Eur. Phys. J. C* **60** (2009) 359 [*Erratum ibid.* **C 61** (2009) 353] [[INSPIRE](#)].
- [40] T. Sjöstrand, S. Mrenna and P.Z. Skands, *PYTHIA 6.4 physics and manual*, *JHEP* **05** (2006) 026 [[hep-ph/0603175](#)] [[INSPIRE](#)].
- [41] R. Field, *Early LHC underlying event data — Findings and surprises*, [arXiv:1010.3558](#) [[INSPIRE](#)].
- [42] I.P. Lokhtin and A.M. Snigirev, *A model of jet quenching in ultrarelativistic heavy ion collisions and high- p_T hadron spectra at RHIC*, *Eur. Phys. J. C* **45** (2006) 211 [[hep-ph/0506189](#)] [[INSPIRE](#)].
- [43] GEANT4 collaboration, S. Agostinelli et al., *GEANT4: a simulation toolkit*, *Nucl. Instrum. Meth. A* **506** (2003) 250 [[INSPIRE](#)].
- [44] CMS collaboration, *Underlying-event subtraction for particle flow*, CMS-DP-2013-018 (2013).
- [45] G. H. Golub and C. Reinsch, *Singular value decomposition and least squares solutions*, *Numerische Math.* **14** (1970) 403.
- [46] CMS collaboration, *Determination of jet energy calibration and transverse momentum resolution in CMS*, 2011 *JINST* **6** P11002 [[arXiv:1107.4277](#)] [[INSPIRE](#)].
- [47] Y. Tachibana and T. Hirano, *Momentum transport away from a jet in an expanding nuclear medium*, *Phys. Rev. C* **90** (2014) 021902 [[arXiv:1402.6469](#)] [[INSPIRE](#)].
- [48] J.-P. Blaizot, L. Fister and Y. Mehtar-Tani, *Angular distribution of medium-induced QCD cascades*, *Nucl. Phys. A* **940** (2015) 67 [[arXiv:1409.6202](#)] [[INSPIRE](#)].
- [49] E. Iancu and B. Wu, *Thermalization of mini-jets in a quark-gluon plasma*, *JHEP* **10** (2015) 155 [[arXiv:1506.07871](#)] [[INSPIRE](#)].
- [50] L. Fister and E. Iancu, *Medium-induced jet evolution: wave turbulence and energy loss*, *JHEP* **03** (2015) 082 [[arXiv:1409.2010](#)] [[INSPIRE](#)].
- [51] J.-P. Blaizot, Y. Mehtar-Tani and M.A.C. Torres, *Angular structure of the in-medium QCD cascade*, *Phys. Rev. Lett.* **114** (2015) 222002 [[arXiv:1407.0326](#)] [[INSPIRE](#)].
- [52] L. Apolinario, N. Armesto and L. Cunqueiro, *Background subtraction and jet quenching on jet reconstruction*, *Nucl. Phys. A* **910-911** (2013) 433 [[arXiv:1207.6587](#)] [[INSPIRE](#)].
- [53] N. Armesto, L. Cunqueiro and C.A. Salgado, *Q-PYTHIA: a medium-modified implementation of final state radiation*, *Eur. Phys. J. C* **63** (2009) 679 [[arXiv:0907.1014](#)] [[INSPIRE](#)].

- [54] M. Dasgupta, F. Dreyer, G.P. Salam and G. Soyez, *Small-radius jets to all orders in QCD*, *JHEP* **04** (2015) 039 [[arXiv:1411.5182](#)] [[INSPIRE](#)].
- [55] M. Cacciari, J. Rojo, G.P. Salam and G. Soyez, *Quantifying the performance of jet definitions for kinematic reconstruction at the LHC*, *JHEP* **12** (2008) 032 [[arXiv:0810.1304](#)] [[INSPIRE](#)].
- [56] ATLAS collaboration, *Measurement of the jet radius and transverse momentum dependence of inclusive jet suppression in lead-lead collisions at $\sqrt{s_{NN}} = 2.76$ TeV with the ATLAS detector*, *Phys. Lett. B* **719** (2013) 220 [[arXiv:1208.1967](#)] [[INSPIRE](#)].

The CMS collaboration

Yerevan Physics Institute, Yerevan, Armenia

V. Khachatryan, A.M. Sirunyan, A. Tumasyan

Institut für Hochenergiephysik der OeAW, Wien, Austria

W. Adam, E. Asilar, T. Bergauer, J. Brandstetter, E. Brondolin, M. Dragicevic, J. Erö, M. Flechl, M. Friedl, R. Frühwirth¹, V.M. Ghete, C. Hartl, N. Hörmann, J. Hrubec, M. Jeitler¹, V. Knünz, A. König, M. Krammer¹, I. Krätschmer, D. Liko, T. Matsushita, I. Mikulec, D. Rabady², B. Rahbaran, H. Rohringer, J. Schieck¹, R. Schöfbeck, J. Strauss, W. Treberer-Treberspurg, W. Waltenberger, C.-E. Wulz¹

National Centre for Particle and High Energy Physics, Minsk, Belarus

V. Mossolov, N. Shumeiko, J. Suarez Gonzalez

Universiteit Antwerpen, Antwerpen, Belgium

S. Alderweireldt, T. Cornelis, E.A. De Wolf, X. Janssen, A. Knutsson, J. Lauwers, S. Luyckx, M. Van De Klundert, H. Van Haevermaet, P. Van Mechelen, N. Van Remortel, A. Van Spilbeeck

Vrije Universiteit Brussel, Brussel, Belgium

S. Abu Zeid, F. Blekman, J. D'Hondt, N. Daci, I. De Bruyn, K. Deroover, N. Heracleous, J. Keaveney, S. Lowette, L. Moreels, A. Olbrechts, Q. Python, D. Strom, S. Tavernier, W. Van Doninck, P. Van Mulders, G.P. Van Onsem, I. Van Parijs

Université Libre de Bruxelles, Bruxelles, Belgium

P. Barria, H. Brun, C. Caillol, B. Clerboux, G. De Lentdecker, G. Fasanella, L. Favart, A. Grebenyuk, G. Karapostoli, T. Lenzi, A. Léonard, T. Maerschalk, A. Marinov, L. Perniè, A. Randle-conde, T. Seva, C. Vander Velde, P. Vanlaer, R. Yonamine, F. Zenoni, F. Zhang³

Ghent University, Ghent, Belgium

K. Beernaert, L. Benucci, A. Cimmino, S. Crucy, D. Dobur, A. Fagot, G. Garcia, M. Gul, J. Mccartin, A.A. Ocampo Rios, D. Poyraz, D. Ryckbosch, S. Salva, M. Sigamani, M. Tytgat, W. Van Driessche, E. Yazgan, N. Zaganidis

Université Catholique de Louvain, Louvain-la-Neuve, Belgium

S. Basegmez, C. Beluffi⁴, O. Bondu, S. Brochet, G. Bruno, A. Caudron, L. Ceard, G.G. Da Silveira, C. Delaere, D. Favart, L. Forthomme, A. Giammanco⁵, J. Hollar, A. Jafari, P. Jez, M. Komm, V. Lemaitre, A. Mertens, M. Musich, C. Nuttens, L. Perrini, A. Pin, K. Piotrkowski, A. Popov⁶, L. Quertenmont, M. Selvaggi, M. Vidal Marono

Université de Mons, Mons, Belgium

N. Belyi, G.H. Hammad

Centro Brasileiro de Pesquisas Fisicas, Rio de Janeiro, Brazil

W.L. Aldá Júnior, F.L. Alves, G.A. Alves, L. Brito, M. Correa Martins Junior, M. Hamer, C. Hensel, C. Mora Herrera, A. Moraes, M.E. Pol, P. Rebello Teles

Universidade do Estado do Rio de Janeiro, Rio de Janeiro, Brazil

E. Belchior Batista Das Chagas, W. Carvalho, J. Chinellato⁷, A. Custódio, E.M. Da Costa, D. De Jesus Damiao, C. De Oliveira Martins, S. Fonseca De Souza, L.M. Huertas Guativa, H. Malbouisson, D. Matos Figueiredo, L. Mundim, H. Nogima, W.L. Prado Da Silva, A. Santoro, A. Sznajder, E.J. Tonelli Manganote⁷, A. Vilela Pereira

Universidade Estadual Paulista ^a, Universidade Federal do ABC ^b, São Paulo, Brazil

S. Ahuja^a, C.A. Bernardes^b, A. De Souza Santos^b, S. Dogra^a, T.R. Fernandez Perez Tomei^a, E.M. Gregores^b, P.G. Mercadante^b, C.S. Moon^{a,8}, S.F. Novaes^a, Sandra S. Padula^a, D. Romero Abad, J.C. Ruiz Vargas

Institute for Nuclear Research and Nuclear Energy, Sofia, Bulgaria

A. Aleksandrov, R. Hadjiiska, P. Iaydjiev, M. Rodozov, S. Stoykova, G. Sultanov, M. Vutova

University of Sofia, Sofia, Bulgaria

A. Dimitrov, I. Glushkov, L. Litov, B. Pavlov, P. Petkov

Institute of High Energy Physics, Beijing, China

M. Ahmad, J.G. Bian, G.M. Chen, H.S. Chen, M. Chen, T. Cheng, R. Du, C.H. Jiang, R. Plestina⁹, F. Romeo, S.M. Shaheen, A. Spiezia, J. Tao, C. Wang, Z. Wang, H. Zhang

State Key Laboratory of Nuclear Physics and Technology, Peking University, Beijing, China

C. Asawatrangkuldee, Y. Ban, Q. Li, S. Liu, Y. Mao, S.J. Qian, D. Wang, Z. Xu

Universidad de Los Andes, Bogota, Colombia

C. Avila, A. Cabrera, L.F. Chaparro Sierra, C. Florez, J.P. Gomez, B. Gomez Moreno, J.C. Sanabria

University of Split, Faculty of Electrical Engineering, Mechanical Engineering and Naval Architecture, Split, Croatia

N. Godinovic, D. Lelas, I. Puljak, P.M. Ribeiro Cipriano

University of Split, Faculty of Science, Split, Croatia

Z. Antunovic, M. Kovac

Institute Rudjer Boskovic, Zagreb, Croatia

V. Brigljevic, K. Kadija, J. Luetic, S. Micanovic, L. Sudic

University of Cyprus, Nicosia, Cyprus

A. Attikis, G. Mavromanolakis, J. Mousa, C. Nicolaou, F. Ptochos, P.A. Razis, H. Rykaczewski

Charles University, Prague, Czech Republic

M. Bodlak, M. Finger¹⁰, M. Finger Jr.¹⁰

**Academy of Scientific Research and Technology of the Arab Republic of Egypt,
Egyptian Network of High Energy Physics, Cairo, Egypt**

A.A. Abdelalim^{11,12}, A. Awad, M. El Sawy^{13,14}, A. Mahrous¹¹, A. Radi^{14,15}

National Institute of Chemical Physics and Biophysics, Tallinn, Estonia

B. Calpas, M. Kadastik, M. Murumaa, M. Raidal, A. Tiko, C. Veelken

Department of Physics, University of Helsinki, Helsinki, Finland

P. Eerola, J. Pekkanen, M. Voutilainen

Helsinki Institute of Physics, Helsinki, Finland

J. Härkönen, V. Karimäki, R. Kinnunen, T. Lampén, K. Lassila-Perini, S. Lehti, T. Lindén, P. Luukka, T. Mäenpää, T. Peltola, E. Tuominen, J. Tuominiemi, E. Tuovinen, L. Wendland

Lappeenranta University of Technology, Lappeenranta, Finland

J. Talvitie, T. Tuuva

DSM/IRFU, CEA/Saclay, Gif-sur-Yvette, France

M. Besancon, F. Couderc, M. Dejardin, D. Denegri, B. Fabbro, J.L. Faure, C. Favaro, F. Ferri, S. Ganjour, A. Givernaud, P. Gras, G. Hamel de Monchenault, P. Jarry, E. Locci, M. Machet, J. Malcles, J. Rander, A. Rosowsky, M. Titov, A. Zghiche

Laboratoire Leprince-Ringuet, Ecole Polytechnique, IN2P3-CNRS, Palaiseau, France

I. Antropov, S. Baffioni, F. Beaudette, P. Busson, L. Cadamuro, E. Chapon, C. Charlot, T. Dahms, O. Davignon, N. Filipovic, A. Florent, R. Granier de Cassagnac, S. Lisniak, L. Mastrolorenzo, P. Miné, I.N. Naranjo, M. Nguyen, C. Ochando, G. Ortona, P. Paganini, P. Pigard, S. Regnard, R. Salerno, J.B. Sauvan, Y. Sirois, T. Strebler, Y. Yilmaz, A. Zabi

Institut Pluridisciplinaire Hubert Curien, Université de Strasbourg, Université de Haute Alsace Mulhouse, CNRS/IN2P3, Strasbourg, France

J.-L. Agram¹⁶, J. Andrea, A. Aubin, D. Bloch, J.-M. Brom, M. Buttignol, E.C. Chabert, N. Chanon, C. Collard, E. Conte¹⁶, X. Coubez, J.-C. Fontaine¹⁶, D. Gelé, U. Goerlach, C. Goetzmann, A.-C. Le Bihan, J.A. Merlin², K. Skovpen, P. Van Hove

Centre de Calcul de l'Institut National de Physique Nucleaire et de Physique des Particules, CNRS/IN2P3, Villeurbanne, France

S. Gadrat

Université de Lyon, Université Claude Bernard Lyon 1, CNRS-IN2P3, Institut de Physique Nucléaire de Lyon, Villeurbanne, France

S. Beauceron, C. Bernet, G. Boudoul, E. Bouvier, C.A. Carrillo Montoya, R. Chierici, D. Contardo, B. Courbon, P. Depasse, H. El Mamouni, J. Fan, J. Fay, S. Gascon, M. Gouzevitch, B. Ille, F. Lagarde, I.B. Laktineh, M. Lethuillier, L. Mirabito, A.L. Pequegnot, S. Perries, J.D. Ruiz Alvarez, D. Sabes, L. Sgandurra, V. Sordini, M. Vander Donckt, P. Verdier, S. Viret

Georgian Technical University, Tbilisi, Georgia

T. Toriashvili¹⁷

Tbilisi State University, Tbilisi, Georgia

Z. Tsamalaidze¹⁰

RWTH Aachen University, I. Physikalisches Institut, Aachen, Germany

C. Autermann, S. Beranek, M. Edelhoff, L. Feld, A. Heister, M.K. Kiesel, K. Klein, M. Lipinski, A. Ostapchuk, M. Preuten, F. Raupach, S. Schael, J.F. Schulte, T. Verlage, H. Weber, B. Wittmer, V. Zhukov⁶

RWTH Aachen University, III. Physikalisches Institut A, Aachen, Germany

M. Ata, M. Brodski, E. Dietz-Laursonn, D. Duchardt, M. Endres, M. Erdmann, S. Erdweg, T. Esch, R. Fischer, A. Güth, T. Hebbeker, C. Heidemann, K. Hoepfner, S. Knutzen, P. Kreuzer, M. Merschmeyer, A. Meyer, P. Millet, M. Olschewski, K. Padeken, P. Papacz, T. Pook, M. Radziej, H. Reithler, M. Rieger, F. Scheuch, L. Sonnenschein, D. Teysier, S. Thüer

RWTH Aachen University, III. Physikalisches Institut B, Aachen, Germany

V. Cherepanov, Y. Erdogan, G. Flügge, H. Geenen, M. Geisler, F. Hoehle, B. Kargoll, T. Kress, Y. Kuessel, A. Künsken, J. Lingemann, A. Nehr Korn, A. Nowack, I.M. Nugent, C. Pistone, O. Pooth, A. Stahl

Deutsches Elektronen-Synchrotron, Hamburg, Germany

M. Aldaya Martin, I. Asin, N. Bartosik, O. Behnke, U. Behrens, A.J. Bell, K. Borras¹⁸, A. Burgmeier, A. Campbell, S. Choudhury¹⁹, F. Costanza, C. Diez Pardos, G. Dolinska, S. Dooling, T. Dorland, G. Eckerlin, D. Eckstein, T. Eichhorn, G. Flucke, E. Gallo²⁰, J. Garay Garcia, A. Geiser, A. Gizhko, P. Gunnellini, J. Hauk, M. Hempel²¹, H. Jung, A. Kalogeropoulos, O. Karacheban²¹, M. Kasemann, P. Katsas, J. Kieseler, C. Kleinwort, I. Korol, W. Lange, J. Leonard, K. Lipka, A. Lobanov, W. Lohmann²¹, R. Mankel, I. Marfin²¹, I.-A. Melzer-Pellmann, A.B. Meyer, G. Mittag, J. Mnich, A. Mussgiller, S. Naumann-Emme, A. Nayak, E. Ntomari, H. Perrey, D. Pitzl, R. Placakyte, A. Raspereza, B. Roland, M.Ö. Sahin, P. Saxena, T. Schoerner-Sadenius, M. Schröder, C. Seitz, S. Spannagel, K.D. Trippkewitz, R. Walsh, C. Wissing

University of Hamburg, Hamburg, Germany

V. Blobel, M. Centis Vignali, A.R. Draeger, J. Erfle, E. Garutti, K. Goebel, D. Gonzalez, M. Görner, J. Haller, M. Hoffmann, R.S. Höing, A. Junkes, R. Klanner, R. Kogler, N. Kovalchuk, T. Lapsien, T. Lenz, I. Marchesini, D. Marconi, M. Meyer, D. Nowatschin, J. Ott, F. Pantaleo², T. Peiffer, A. Perieanu, N. Pietsch, J. Poehlsen, D. Rathjens, C. Sander, C. Scharf, H. Schettler, P. Schleper, E. Schlieckau, A. Schmidt, J. Schwandt, V. Sola, H. Stadie, G. Steinbrück, H. Tholen, D. Troendle, E. Usai, L. Vanelderen, A. Vanhoefer, B. Vormwald

Institut für Experimentelle Kernphysik, Karlsruhe, Germany

M. Akbiyik, C. Barth, C. Baus, J. Berger, C. Böser, E. Butz, T. Chwalek, F. Colombo, W. De Boer, A. Descroix, A. Dierlamm, S. Fink, F. Frensch, R. Friese, M. Gif-

fels, A. Gilbert, D. Haitz, F. Hartmann², S.M. Heindl, U. Husemann, I. Katkov⁶, A. Kornmayer², P. Lobelle Pardo, B. Maier, H. Mildner, M.U. Mozer, T. Müller, Th. Müller, M. Plagge, G. Quast, K. Rabbertz, S. Röcker, F. Roscher, G. Sieber, H.J. Simonis, F.M. Stober, R. Ulrich, J. Wagner-Kuhr, S. Wayand, M. Weber, T. Weiler, C. Wöhrmann, R. Wolf

Institute of Nuclear and Particle Physics (INPP), NCSR Demokritos, Aghia Paraskevi, Greece

G. Anagnostou, G. Daskalakis, T. Gerasis, V.A. Giakoumopoulou, A. Kyriakis, D. Loukas, A. Psallidas, I. Topsis-Giotis

University of Athens, Athens, Greece

A. Agapitos, S. Kesisoglou, A. Panagiotou, N. Saoulidou, E. Tziaferi

University of Ioánnina, Ioánnina, Greece

I. Evangelou, G. Flouris, C. Foudas, P. Kokkas, N. Loukas, N. Manthos, I. Papadopoulos, E. Paradas, J. Strologas

Wigner Research Centre for Physics, Budapest, Hungary

G. Bencze, C. Hajdu, A. Hazi, P. Hidas, D. Horvath²², F. Sikler, V. Veszpremi, G. Vesztergombi²³, A.J. Zsigmond

Institute of Nuclear Research ATOMKI, Debrecen, Hungary

N. Beni, S. Czellar, J. Karancsi²⁴, J. Molnar, Z. Szillasi²

University of Debrecen, Debrecen, Hungary

M. Bartók²⁵, A. Makovec, P. Raics, Z.L. Trocsanyi, B. Ujvari

National Institute of Science Education and Research, Bhubaneswar, India

P. Mal, K. Mandal, D.K. Sahoo, N. Sahoo, S.K. Swain

Panjab University, Chandigarh, India

S. Bansal, S.B. Beri, V. Bhatnagar, R. Chawla, R. Gupta, U. Bhawandeep, A.K. Kalsi, A. Kaur, M. Kaur, R. Kumar, A. Mehta, M. Mittal, J.B. Singh, G. Walia

University of Delhi, Delhi, India

Ashok Kumar, A. Bhardwaj, B.C. Choudhary, R.B. Garg, A. Kumar, S. Malhotra, M. Naimuddin, N. Nishu, K. Ranjan, R. Sharma, V. Sharma

Saha Institute of Nuclear Physics, Kolkata, India

S. Bhattacharya, K. Chatterjee, S. Dey, S. Dutta, Sa. Jain, N. Majumdar, A. Modak, K. Mondal, S. Mukherjee, S. Mukhopadhyay, A. Roy, D. Roy, S. Roy Chowdhury, S. Sarkar, M. Sharan

Bhabha Atomic Research Centre, Mumbai, India

A. Abdulsalam, R. Chudasama, D. Dutta, V. Jha, V. Kumar, A.K. Mohanty², L.M. Pant, P. Shukla, A. Topkar

Tata Institute of Fundamental Research, Mumbai, India

T. Aziz, S. Banerjee, S. Bhowmik²⁶, R.M. Chatterjee, R.K. Dewanjee, S. Dugad, S. Ganguly, S. Ghosh, M. Guchait, A. Gurtu²⁷, G. Kole, S. Kumar, B. Mahakud, M. Maity²⁶, G. Majumder, K. Mazumdar, S. Mitra, G.B. Mohanty, B. Parida, T. Sarkar²⁶, N. Sur, B. Sutar, N. Wickramage²⁸

Indian Institute of Science Education and Research (IISER), Pune, India

S. Chauhan, S. Dube, K. Kothekar, S. Sharma

Institute for Research in Fundamental Sciences (IPM), Tehran, Iran

H. Bakhshiansohi, H. Behnamian, S.M. Etesami²⁹, A. Fahim³⁰, R. Goldouzian, M. Khakzad, M. Mohammadi Najafabadi, M. Naseri, S. Paktinat Mehdiabadi, F. Rezaei Hosseinabadi, B. Safarzadeh³¹, M. Zeinali

University College Dublin, Dublin, Ireland

M. Felcini, M. Grunewald

INFN Sezione di Bari ^a, Università di Bari ^b, Politecnico di Bari ^c, Bari, Italy

M. Abbrescia^{a,b}, C. Calabria^{a,b}, C. Caputo^{a,b}, A. Colaleo^a, D. Creanza^{a,c}, L. Cristella^{a,b}, N. De Filippis^{a,c}, M. De Palma^{a,b}, L. Fiore^a, G. Iaselli^{a,c}, G. Maggi^{a,c}, M. Maggi^a, G. Miniello^{a,b}, S. My^{a,c}, S. Nuzzo^{a,b}, A. Pompili^{a,b}, G. Pugliese^{a,c}, R. Radogna^{a,b}, A. Ranieri^a, G. Selvaggi^{a,b}, L. Silvestris^{a,2}, R. Venditti^{a,b}, P. Verwilligen^a

INFN Sezione di Bologna ^a, Università di Bologna ^b, Bologna, Italy

G. Abbiendi^a, C. Battilana², A.C. Benvenuti^a, D. Bonacorsi^{a,b}, S. Braibant-Giacomelli^{a,b}, L. Brigliadori^{a,b}, R. Campanini^{a,b}, P. Capiluppi^{a,b}, A. Castro^{a,b}, F.R. Cavallo^a, S.S. Chhibra^{a,b}, G. Codispoti^{a,b}, M. Cuffiani^{a,b}, G.M. Dallavalle^a, F. Fabbri^a, A. Fanfani^{a,b}, D. Fasanella^{a,b}, P. Giacomelli^a, C. Grandi^a, L. Guiducci^{a,b}, S. Marcellini^a, G. Masetti^a, A. Montanari^a, F.L. Navarria^{a,b}, A. Perrotta^a, A.M. Rossi^{a,b}, T. Rovelli^{a,b}, G.P. Siroli^{a,b}, N. Tosi^{a,b,2}, R. Travaglini^{a,b}

INFN Sezione di Catania ^a, Università di Catania ^b, Catania, Italy

G. Cappello^a, M. Chiorboli^{a,b}, S. Costa^{a,b}, A. Di Mattia^a, F. Giordano^{a,b}, R. Potenza^{a,b}, A. Tricomi^{a,b}, C. Tuve^{a,b}

INFN Sezione di Firenze ^a, Università di Firenze ^b, Firenze, Italy

G. Barbagli^a, V. Ciulli^{a,b}, C. Civinini^a, R. D'Alessandro^{a,b}, E. Focardi^{a,b}, S. Gonzi^{a,b}, V. Gori^{a,b}, P. Lenzi^{a,b}, M. Meschini^a, S. Paoletti^a, G. Sguazzoni^a, A. Tropiano^{a,b}, L. Viliani^{a,b,2}

INFN Laboratori Nazionali di Frascati, Frascati, Italy

L. Benussi, S. Bianco, F. Fabbri, D. Piccolo, F. Primavera²

INFN Sezione di Genova ^a, Università di Genova ^b, Genova, Italy

V. Calvelli^{a,b}, F. Ferro^a, M. Lo Vetere^{a,b}, M.R. Monge^{a,b}, E. Robutti^a, S. Tosi^{a,b}

INFN Sezione di Milano-Bicocca ^a, Università di Milano-Bicocca ^b, Milano, Italy

L. Brianza, M.E. Dinardo^{a,b}, S. Fiorendi^{a,b}, S. Gennai^a, R. Gerosa^{a,b}, A. Ghezzi^{a,b}, P. Govoni^{a,b}, S. Malvezzi^a, R.A. Manzoni^{a,b,2}, B. Marzocchi^{a,b,2}, D. Menasce^a, L. Moroni^a, M. Paganoni^{a,b}, D. Pedrini^a, S. Ragazzi^{a,b}, N. Redaelli^a, T. Tabarelli de Fatis^{a,b}

INFN Sezione di Napoli ^a, Università di Napoli 'Federico II' ^b, Napoli, Italy, Università della Basilicata ^c, Potenza, Italy, Università G. Marconi ^d, Roma, Italy

S. Buontempo^a, N. Cavallo^{a,c}, S. Di Guida^{a,d,2}, M. Esposito^{a,b}, F. Fabozzi^{a,c}, A.O.M. Iorio^{a,b}, G. Lanza^a, L. Lista^a, S. Meola^{a,d,2}, M. Merola^a, P. Paolucci^{a,2}, C. Sciacca^{a,b}, F. Thyssen

INFN Sezione di Padova ^a, Università di Padova ^b, Padova, Italy, Università di Trento ^c, Trento, Italy

P. Azzi^{a,2}, N. Bacchetta^a, L. Benato^{a,b}, A. Boletti^{a,b}, A. Branca^{a,b}, M. Dall'Osso^{a,b,2}, T. Dorigo^a, F. Fanzago^a, F. Gonella^a, A. Gozzelino^a, K. Kanishchev^{a,c}, M. Margoni^{a,b}, G. Maron^{a,32}, A.T. Meneguzzo^{a,b}, M. Michelotto^a, F. Montecassiano^a, M. Passaseo^a, J. Pazzini^{a,b,2}, M. Pegoraro^a, N. Pozzobon^{a,b}, P. Ronchese^{a,b}, F. Simonetto^{a,b}, E. Torassa^a, M. Tosi^{a,b}, S. Vanini^{a,b}, S. Ventura^a, M. Zanetti, P. Zotto^{a,b}, A. Zucchetta^{a,b,2}

INFN Sezione di Pavia ^a, Università di Pavia ^b, Pavia, Italy

A. Braghieri^a, A. Magnani^a, P. Montagna^{a,b}, S.P. Ratti^{a,b}, V. Re^a, C. Riccardi^{a,b}, P. Salvini^a, I. Vai^a, P. Vitulo^{a,b}

INFN Sezione di Perugia ^a, Università di Perugia ^b, Perugia, Italy

L. Alunni Solestizi^{a,b}, M. Biasini^{a,b}, G.M. Bilei^a, D. Ciangottini^{a,b,2}, L. Fanò^{a,b}, P. Lariccia^{a,b}, G. Mantovani^{a,b}, M. Menichelli^a, A. Saha^a, A. Santocchia^{a,b}

INFN Sezione di Pisa ^a, Università di Pisa ^b, Scuola Normale Superiore di Pisa ^c, Pisa, Italy

K. Androsov^{a,33}, P. Azzurri^{a,2}, G. Bagliesi^a, J. Bernardini^a, T. Boccali^a, R. Castaldi^a, M.A. Ciocci^{a,33}, R. Dell'Orso^a, S. Donato^{a,c,2}, G. Fedi, L. Foà^{a,c†}, A. Giassi^a, M.T. Grippo^{a,33}, F. Ligabue^{a,c}, T. Lomtadze^a, L. Martini^{a,b}, A. Messineo^{a,b}, F. Palla^a, A. Rizzi^{a,b}, A. Savoy-Navarro^{a,34}, A.T. Serban^a, P. Spagnolo^a, R. Tenchini^a, G. Tonelli^{a,b}, A. Venturi^a, P.G. Verdini^a

INFN Sezione di Roma ^a, Università di Roma ^b, Roma, Italy

L. Barone^{a,b}, F. Cavallari^a, G. D'imperio^{a,b,2}, D. Del Re^{a,b,2}, M. Diemoz^a, S. Gelli^{a,b}, C. Jorda^a, E. Longo^{a,b}, F. Margaroli^{a,b}, P. Meridiani^a, G. Organtini^{a,b}, R. Paramatti^a, F. Preiato^{a,b}, S. Rahatlou^{a,b}, C. Rovelli^a, F. Santanastasio^{a,b}, P. Traczyk^{a,b,2}

INFN Sezione di Torino ^a, Università di Torino ^b, Torino, Italy, Università del Piemonte Orientale ^c, Novara, Italy

N. Amapane^{a,b}, R. Arcidiacono^{a,c,2}, S. Argiro^{a,b}, M. Arneodo^{a,c}, R. Bellan^{a,b}, C. Biino^a, N. Cartiglia^a, M. Costa^{a,b}, R. Covarelli^{a,b}, A. Degano^{a,b}, N. Demaria^a, L. Finco^{a,b,2}, B. Kiani^{a,b}, C. Mariotti^a, S. Maselli^a, E. Migliore^{a,b}, V. Monaco^{a,b}, E. Monteil^{a,b},

M.M. Obertino^{a,b}, L. Pacher^{a,b}, N. Pastrone^a, M. Pelliccioni^a, G.L. Pinna Angioni^{a,b},
F. Ravera^{a,b}, A. Romero^{a,b}, M. Ruspa^{a,c}, R. Sacchi^{a,b}, A. Solano^{a,b}, A. Staiano^a

INFN Sezione di Trieste^a, Università di Trieste^b, Trieste, Italy

S. Belforte^a, V. Candelise^{a,b,2}, M. Casarsa^a, F. Cossutti^a, G. Della Ricca^{a,b}, B. Gobbo^a,
C. La Licata^{a,b}, M. Marone^{a,b}, A. Schizzi^{a,b}, A. Zanetti^a

Kangwon National University, Chunchon, Korea

A. Kropivnitskaya, S.K. Nam

Kyungpook National University, Daegu, Korea

D.H. Kim, G.N. Kim, M.S. Kim, D.J. Kong, S. Lee, Y.D. Oh, A. Sakharov, D.C. Son

Chonbuk National University, Jeonju, Korea

J.A. Brochero Cifuentes, H. Kim, T.J. Kim

**Chonnam National University, Institute for Universe and Elementary Particles,
Kwangju, Korea**

S. Song

Korea University, Seoul, Korea

S. Choi, Y. Go, D. Gyun, B. Hong, M. Jo, H. Kim, Y. Kim, B. Lee, K. Lee, K.S. Lee,
S. Lee, S.K. Park, Y. Roh

Seoul National University, Seoul, Korea

H.D. Yoo

University of Seoul, Seoul, Korea

M. Choi, H. Kim, J.H. Kim, J.S.H. Lee, I.C. Park, G. Ryu, M.S. Ryu

Sungkyunkwan University, Suwon, Korea

Y. Choi, J. Goh, D. Kim, E. Kwon, J. Lee, I. Yu

Vilnius University, Vilnius, Lithuania

V. Dudenas, A. Juodagalvis, J. Vaitkus

**National Centre for Particle Physics, Universiti Malaya, Kuala Lumpur,
Malaysia**

I. Ahmed, Z.A. Ibrahim, J.R. Komaragiri, M.A.B. Md Ali³⁵, F. Mohamad Idris³⁶,
W.A.T. Wan Abdullah, M.N. Yusli

Centro de Investigacion y de Estudios Avanzados del IPN, Mexico City, Mexico

E. Casimiro Linares, H. Castilla-Valdez, E. De La Cruz-Burelo, I. Heredia-De La Cruz³⁷,
A. Hernandez-Almada, R. Lopez-Fernandez, A. Sanchez-Hernandez

Universidad Iberoamericana, Mexico City, Mexico

S. Carrillo Moreno, F. Vazquez Valencia

Benemerita Universidad Autonoma de Puebla, Puebla, Mexico

I. Pedraza, H.A. Salazar Ibarguen

Universidad Autónoma de San Luis Potosí, San Luis Potosí, Mexico

A. Morelos Pineda

University of Auckland, Auckland, New Zealand

D. Krofcheck

University of Canterbury, Christchurch, New Zealand

P.H. Butler

National Centre for Physics, Quaid-I-Azam University, Islamabad, Pakistan

A. Ahmad, M. Ahmad, Q. Hassan, H.R. Hoorani, W.A. Khan, T. Khurshid, M. Shoaib

National Centre for Nuclear Research, Swierk, Poland

H. Bialkowska, M. Bluj, B. Boimska, T. Frueboes, M. Górski, M. Kazana, K. Nawrocki, K. Romanowska-Rybinska, M. Szleper, P. Zalewski

Institute of Experimental Physics, Faculty of Physics, University of Warsaw, Warsaw, Poland

G. Brona, K. Bunkowski, A. Byszuk³⁸, K. Doroba, A. Kalinowski, M. Konecki, J. Krolikowski, M. Misiura, M. Olszewski, M. Walczak

Laboratório de Instrumentação e Física Experimental de Partículas, Lisboa, Portugal

P. Bargassa, C. Beirão Da Cruz E Silva, A. Di Francesco, P. Faccioli, P.G. Ferreira Parracho, M. Gallinaro, N. Leonardo, L. Lloret Iglesias, F. Nguyen, J. Rodrigues Antunes, J. Seixas, O. Toldaiev, D. Vadrucio, J. Varela, P. Vischia

Joint Institute for Nuclear Research, Dubna, Russia

S. Afanasiev, P. Bunin, M. Gavrilenko, I. Golutvin, I. Gorbunov, A. Kamenev, V. Karjavin, V. Konoplyanikov, A. Lanev, A. Malakhov, V. Matveev^{39,40}, P. Moiseenz, V. Palichik, V. Perelygin, S. Shmatov, S. Shulha, N. Skatchkov, V. Smirnov, A. Zarubin

Petersburg Nuclear Physics Institute, Gatchina (St. Petersburg), Russia

V. Golovtsov, Y. Ivanov, V. Kim⁴¹, E. Kuznetsova, P. Levchenko, V. Murzin, V. Oreshkin, I. Smirnov, V. Sulimov, L. Uvarov, S. Vavilov, A. Vorobyev

Institute for Nuclear Research, Moscow, Russia

Yu. Andreev, A. Dermenev, S. Gninenko, N. Golubev, A. Karneyeu, M. Kirsanov, N. Krasnikov, A. Pashenkov, D. Tlisov, A. Toropin

Institute for Theoretical and Experimental Physics, Moscow, Russia

V. Epshteyn, V. Gavrilov, N. Lychkovskaya, V. Popov, I. Pozdnyakov, G. Safronov, A. Spiridonov, E. Vlasov, A. Zhokin

National Research Nuclear University 'Moscow Engineering Physics Institute' (MEPhI), Moscow, Russia

A. Bylinkin

P.N. Lebedev Physical Institute, Moscow, Russia

V. Andreev, M. Azarkin⁴⁰, I. Dremin⁴⁰, M. Kirakosyan, A. Leonidov⁴⁰, G. Mesyats, S.V. Rusakov

Skobeltsyn Institute of Nuclear Physics, Lomonosov Moscow State University, Moscow, Russia

A. Baskakov, A. Belyaev, E. Boos, A. Ershov, A. Gribushin, A. Kaminskiy⁴², O. Kodolova, V. Korotkikh, I. Lokhtin, I. Myagkov, S. Obraztsov, S. Petrushanko, V. Savrin, A. Snigirev, I. Vardanyan

State Research Center of Russian Federation, Institute for High Energy Physics, Protvino, Russia

I. Azhgirey, I. Bayshev, S. Bitioukov, V. Kachanov, A. Kalinin, D. Konstantinov, V. Krychkin, V. Petrov, R. Ryutin, A. Sobol, L. Tourtchanovitch, S. Troshin, N. Tyurin, A. Uzunian, A. Volkov

University of Belgrade, Faculty of Physics and Vinca Institute of Nuclear Sciences, Belgrade, Serbia

P. Adzic⁴³, P. Cirkovic, J. Milosevic, V. Rekovic

Centro de Investigaciones Energéticas Medioambientales y Tecnológicas (CIEMAT), Madrid, Spain

J. Alcaraz Maestre, E. Calvo, M. Cerrada, M. Chamizo Llatas, N. Colino, B. De La Cruz, A. Delgado Peris, D. Domínguez Vázquez, A. Escalante Del Valle, C. Fernandez Bedoya, J.P. Fernández Ramos, J. Flix, M.C. Fouz, P. Garcia-Abia, O. Gonzalez Lopez, S. Goy Lopez, J.M. Hernandez, M.I. Josa, E. Navarro De Martino, A. Pérez-Calero Yzquierdo, J. Puerta Pelayo, A. Quintario Olmeda, I. Redondo, L. Romero, J. Santaolalla, M.S. Soares

Universidad Autónoma de Madrid, Madrid, Spain

C. Albajar, J.F. de Trocóniz, M. Missiroli, D. Moran

Universidad de Oviedo, Oviedo, Spain

J. Cuevas, J. Fernandez Menendez, S. Folgueras, I. Gonzalez Caballero, E. Palencia Cortezon, J.M. Vizán García

Instituto de Física de Cantabria (IFCA), CSIC-Universidad de Cantabria, Santander, Spain

I.J. Cabrillo, A. Calderon, J.R. Castiñeiras De Saa, P. De Castro Manzano, M. Fernandez, J. Garcia-Ferrero, G. Gomez, A. Lopez Virto, J. Marco, R. Marco, C. Martinez Rivero, F. Matorras, J. Piedra Gomez, T. Rodrigo, A.Y. Rodríguez-Marrero, A. Ruiz-Jimeno, L. Scodellaro, N. Trevisani, I. Vila, R. Vilar Cortabitarte

CERN, European Organization for Nuclear Research, Geneva, Switzerland

D. Abbaneo, E. Auffray, G. Auzinger, M. Bachtis, P. Baillon, A.H. Ball, D. Barney, A. Benaglia, J. Bendavid, L. Benhabib, J.F. Benitez, G.M. Berruti, P. Bloch, A. Bocci, A. Bonato, C. Botta, H. Breuker, T. Camporesi, R. Castello, G. Cerminara, M. D'Alfonso, D. d'Enterria, A. Dabrowski, V. Daponte, A. David, M. De Gruttola, F. De Guio, A. De

Roeck, S. De Visscher, E. Di Marco⁴⁴, M. Dobson, M. Dordevic, B. Dorney, T. du Pree, D. Duggan, M. Dünser, N. Dupont, A. Elliott-Peisert, G. Franzoni, J. Fulcher, W. Funk, D. Gigi, K. Gill, D. Giordano, M. Girone, F. Glege, R. Guida, S. Gundacker, M. Guthoff, J. Hammer, P. Harris, J. Hegeman, V. Innocente, P. Janot, H. Kirschenmann, M.J. Kortelainen, K. Kousouris, K. Krajczar, P. Lecoq, C. Lourenço, M.T. Lucchini, N. Magini, L. Malgeri, M. Mannelli, A. Martelli, L. Masetti, F. Meijers, S. Mersi, E. Meschi, F. Moortgat, S. Morovic, M. Mulders, M.V. Nemallapudi, H. Neugebauer, S. Orfanelli⁴⁵, L. Orsini, L. Pape, E. Perez, M. Peruzzi, A. Petrilli, G. Petrucciani, A. Pfeiffer, D. Piparo, A. Racz, T. Reis, G. Rolandi⁴⁶, M. Rovere, M. Ruan, H. Sakulin, C. Schäfer, C. Schwick, M. Seidel, A. Sharma, P. Silva, M. Simon, P. Sphicas⁴⁷, J. Steggemann, B. Stieger, M. Stoye, Y. Takahashi, D. Treille, A. Triossi, A. Tsirou, G.I. Veres²³, N. Wardle, H.K. Wöhri, A. Zagozdzińska³⁸, W.D. Zeuner

Paul Scherrer Institut, Villigen, Switzerland

W. Bertl, K. Deiters, W. Erdmann, R. Horisberger, Q. Ingram, H.C. Kaestli, D. Kotlinski, U. Langenegger, D. Renker, T. Rohe

Institute for Particle Physics, ETH Zurich, Zurich, Switzerland

F. Bachmair, L. Bäni, L. Bianchini, B. Casal, G. Dissertori, M. Dittmar, M. Donegà, P. Eller, C. Grab, C. Heidegger, D. Hits, J. Hoss, G. Kasieczka, W. Lustermann, B. Mangano, M. Marionneau, P. Martinez Ruiz del Arbol, M. Masciovecchio, D. Meister, F. Micheli, P. Musella, F. Nessi-Tedaldi, F. Pandolfi, J. Pata, F. Pauss, L. Perrozzi, M. Quittnat, M. Rossini, A. Starodumov⁴⁸, M. Takahashi, V.R. Tavolaro, K. Theofilatos, R. Wallny

Universität Zürich, Zurich, Switzerland

T.K. Aarrestad, C. AMSler⁴⁹, L. Caminada, M.F. Canelli, V. Chiochia, A. De Cosa, C. Galloni, A. Hinzmann, T. Hreus, B. Kilminster, C. Lange, J. Ngadiuba, D. Pinna, P. Robmann, F.J. Ronga, D. Salerno, Y. Yang

National Central University, Chung-Li, Taiwan

M. Cardaci, K.H. Chen, T.H. Doan, Sh. Jain, R. Khurana, M. Konyushikhin, C.M. Kuo, W. Lin, Y.J. Lu, S.S. Yu

National Taiwan University (NTU), Taipei, Taiwan

Arun Kumar, R. Bartek, P. Chang, Y.H. Chang, Y.W. Chang, Y. Chao, K.F. Chen, P.H. Chen, C. Dietz, F. Fiori, U. Grundler, W.-S. Hou, Y. Hsiung, Y.F. Liu, R.-S. Lu, M. Miñano Moya, E. Petrakou, J.f. Tsai, Y.M. Tzeng

Chulalongkorn University, Faculty of Science, Department of Physics, Bangkok, Thailand

B. Asavapibhop, K. Kovitanggoon, G. Singh, N. Srimanobhas, N. Suwonjandee

Cukurova University, Adana, Turkey

A. Adiguzel, S. Cerci⁵⁰, Z.S. Demiroglu, C. Dozen, I. Dumanoglu, S. Girgis, G. Gokbulut, Y. Guler, E. Gurbinar, I. Hos, E.E. Kangal⁵¹, A. Kayis Topaksu, G. Onengut⁵², K. Ozdemir⁵³, S. Ozturk⁵⁴, B. Tali⁵⁰, H. Topakli⁵⁴, M. Vergili, C. Zorbilmez

Middle East Technical University, Physics Department, Ankara, Turkey

I.V. Akin, B. Bilin, S. Bilmis, B. Isildak⁵⁵, G. Karapinar⁵⁶, M. Yalvac, M. Zeyrek

Bogazici University, Istanbul, Turkey

E. Gülmez, M. Kaya⁵⁷, O. Kaya⁵⁸, E.A. Yetkin⁵⁹, T. Yetkin⁶⁰

Istanbul Technical University, Istanbul, Turkey

A. Cakir, K. Cankocak, S. Sen⁶¹, F.I. Vardarli

Institute for Scintillation Materials of National Academy of Science of Ukraine, Kharkov, Ukraine

B. Grynyov

National Scientific Center, Kharkov Institute of Physics and Technology, Kharkov, Ukraine

L. Levchuk, P. Sorokin

University of Bristol, Bristol, United Kingdom

R. Aggleton, F. Ball, L. Beck, J.J. Brooke, E. Clement, D. Cussans, H. Flacher, J. Goldstein, M. Grimes, G.P. Heath, H.F. Heath, J. Jacob, L. Kreczko, C. Lucas, Z. Meng, D.M. Newbold⁶², S. Paramesvaran, A. Poll, T. Sakuma, S. Seif El Nasr-storey, S. Senkin, D. Smith, V.J. Smith

Rutherford Appleton Laboratory, Didcot, United Kingdom

A. Belyaev⁶³, C. Brew, R.M. Brown, L. Calligaris, D. Cieri, D.J.A. Cockerill, J.A. Coughlan, K. Harder, S. Harper, E. Olaiya, D. Petyt, C.H. Shepherd-Themistocleous, A. Thea, I.R. Tomalin, T. Williams, S.D. Worm

Imperial College, London, United Kingdom

M. Baber, R. Bainbridge, O. Buchmuller, A. Bundock, D. Burton, S. Casasso, M. Citron, D. Colling, L. Corpe, N. Cripps, P. Dauncey, G. Davies, A. De Wit, M. Della Negra, P. Dunne, A. Elwood, W. Ferguson, D. Futyan, G. Hall, G. Iles, M. Kenzie, R. Lane, R. Lucas⁶², L. Lyons, A.-M. Magnan, S. Malik, J. Nash, A. Nikitenko⁴⁸, J. Pela, M. Pesaresi, K. Petridis, D.M. Raymond, A. Richards, A. Rose, C. Seez, A. Tapper, K. Uchida, M. Vazquez Acosta⁶⁴, T. Virdee, S.C. Zenz

Brunel University, Uxbridge, United Kingdom

J.E. Cole, P.R. Hobson, A. Khan, P. Kyberd, D. Leggat, D. Leslie, I.D. Reid, P. Symonds, L. Teodorescu, M. Turner

Baylor University, Waco, USA

A. Borzou, K. Call, J. Dittmann, K. Hatakeyama, H. Liu, N. Pastika

The University of Alabama, Tuscaloosa, USA

O. Charaf, S.I. Cooper, C. Henderson, P. Rumerio

Boston University, Boston, USA

D. Arcaro, A. Avetisyan, T. Bose, C. Fantasia, D. Gastler, P. Lawson, D. Rankin, C. Richardson, J. Rohlf, J. St. John, L. Sulak, D. Zou

Brown University, Providence, USA

J. Alimena, E. Berry, S. Bhattacharya, D. Cutts, N. Dhirra, A. Ferapontov, A. Garabedian, J. Hakala, U. Heintz, E. Laird, G. Landsberg, Z. Mao, M. Narain, S. Piperov, S. Sagir, R. Syarif

University of California, Davis, Davis, USA

R. Breedon, G. Breto, M. Calderon De La Barca Sanchez, S. Chauhan, M. Chertok, J. Conway, R. Conway, P.T. Cox, R. Erbacher, M. Gardner, W. Ko, R. Lander, M. Mulhearn, D. Pellett, J. Pilot, F. Ricci-Tam, S. Shalhout, J. Smith, M. Squires, D. Stolp, M. Tripathi, S. Wilbur, R. Yohay

University of California, Los Angeles, USA

R. Cousins, P. Everaerts, C. Farrell, J. Hauser, M. Ignatenko, D. Saltzberg, E. Takasugi, V. Valuev, M. Weber

University of California, Riverside, Riverside, USA

K. Burt, R. Clare, J. Ellison, J.W. Gary, G. Hanson, J. Heilman, M. Ivova PANEVA, P. Jandir, E. Kennedy, F. Lacroix, O.R. Long, A. Luthra, M. Malberti, M. Olmedo Negrete, A. Shrinivas, H. Wei, S. Wimpenny, B. R. Yates

University of California, San Diego, La Jolla, USA

J.G. Branson, G.B. Cerati, S. Cittolin, R.T. D’Agnolo, M. Derdzinski, A. Holzner, R. Kelley, D. Klein, J. Letts, I. Macneill, D. Olivito, S. Padhi, M. Pieri, M. Sani, V. Sharma, S. Simon, M. Tadel, A. Vartak, S. Wasserbaech⁶⁵, C. Welke, F. Würthwein, A. Yagil, G. Zevi Della Porta

University of California, Santa Barbara, Santa Barbara, USA

J. Bradmiller-Feld, C. Campagnari, A. Dishaw, V. Dutta, K. Flowers, M. Franco Sevilla, P. Geffert, C. George, F. Golf, L. Gouskos, J. Gran, J. Incandela, N. Mccoll, S.D. Mullin, J. Richman, D. Stuart, I. Suarez, C. West, J. Yoo

California Institute of Technology, Pasadena, USA

D. Anderson, A. Apresyan, A. Bornheim, J. Bunn, Y. Chen, J. Duarte, A. Mott, H.B. Newman, C. Pena, M. Pierini, M. Spiropulu, J.R. Vlimant, S. Xie, R.Y. Zhu

Carnegie Mellon University, Pittsburgh, USA

M.B. Andrews, V. Azzolini, A. Calamba, B. Carlson, T. Ferguson, M. Paulini, J. Russ, M. Sun, H. Vogel, I. Vorobiev

University of Colorado Boulder, Boulder, USA

J.P. Cumalat, W.T. Ford, A. Gaz, F. Jensen, A. Johnson, M. Krohn, T. Mulholland, U. Nauenberg, K. Stenson, S.R. Wagner

Cornell University, Ithaca, USA

J. Alexander, A. Chatterjee, J. Chaves, J. Chu, S. Dittmer, N. Eggert, N. Mirman, G. Nicolas Kaufman, J.R. Patterson, A. Rinkevicius, A. Ryd, L. Skinnari, L. Soffi, W. Sun, S.M. Tan, W.D. Teo, J. Thom, J. Thompson, J. Tucker, Y. Weng, P. Wittich

Fermi National Accelerator Laboratory, Batavia, USA

S. Abdullin, M. Albrow, G. Apollinari, S. Banerjee, L.A.T. Bauerdick, A. Beretvas, J. Berryhill, P.C. Bhat, G. Bolla, K. Burkett, J.N. Butler, H.W.K. Cheung, F. Chlebana, S. Cihangir, V.D. Elvira, I. Fisk, J. Freeman, E. Gottschalk, L. Gray, D. Green, S. Grünendahl, O. Gutsche, J. Hanlon, D. Hare, R.M. Harris, S. Hasegawa, J. Hirschauer, Z. Hu, B. Jayatilaka, S. Jindariani, M. Johnson, U. Joshi, A.W. Jung, B. Klima, B. Kreis, S. Kwan[†], S. Lammel, J. Linacre, D. Lincoln, R. Lipton, T. Liu, R. Lopes De Sá, J. Lykken, K. Maeshima, J.M. Marraffino, V.I. Martinez Outschoorn, S. Maruyama, D. Mason, P. McBride, P. Merkel, K. Mishra, S. Mrenna, S. Nahn, C. Newman-Holmes, V. O'Dell, K. Pedro, O. Prokofyev, G. Rakness, E. Sexton-Kennedy, A. Soha, W.J. Spalding, L. Spiegel, N. Strobbe, L. Taylor, S. Tkaczyk, N.V. Tran, L. Uplegger, E.W. Vaandering, C. Vernieri, M. Verzocchi, R. Vidal, H.A. Weber, A. Whitbeck, F. Yang

University of Florida, Gainesville, USA

D. Acosta, P. Avery, P. Bortignon, D. Bourilkov, A. Carnes, M. Carver, D. Curry, S. Das, R.D. Field, I.K. Furic, S.V. Gleyzer, J. Hugon, J. Konigsberg, A. Korytov, J.F. Low, P. Ma, K. Matchev, H. Mei, P. Milenovic⁶⁶, G. Mitselmakher, D. Rank, R. Rossin, L. Shchutska, M. Snowball, D. Sperka, N. Terentyev, L. Thomas, J. Wang, S. Wang, J. Yelton

Florida International University, Miami, USA

S. Hewamanage, S. Linn, P. Markowitz, G. Martinez, J.L. Rodriguez

Florida State University, Tallahassee, USA

A. Ackert, J.R. Adams, T. Adams, A. Askew, S. Bein, J. Bochenek, B. Diamond, J. Haas, S. Hagopian, V. Hagopian, K.F. Johnson, A. Khatiwada, H. Prosper, M. Weinberg

Florida Institute of Technology, Melbourne, USA

M.M. Baarmand, V. Bhopatkar, S. Colafranceschi⁶⁷, M. Hohlmann, H. Kalakhety, D. Noonan, T. Roy, F. Yumiceva

University of Illinois at Chicago (UIC), Chicago, USA

M.R. Adams, L. Apanasevich, D. Berry, R.R. Betts, I. Bucinskaite, R. Cavanaugh, O. Evdokimov, L. Gauthier, C.E. Gerber, D.J. Hofman, P. Kurt, C. O'Brien, I.D. Sandoval Gonzalez, C. Silkworth, H. Trauger, P. Turner, N. Varelas, Z. Wu, M. Zakaria

The University of Iowa, Iowa City, USA

B. Bilki⁶⁸, W. Clarida, K. Dilsiz, S. Durgut, R.P. Gandrajula, M. Haytmyradov, V. Khristenko, J.-P. Merlo, H. Mermerkaya⁶⁹, A. Mestvirishvili, A. Moeller, J. Nachtman, H. Ogul, Y. Onel, F. Ozok⁵⁹, A. Penzo, C. Snyder, E. Tiras, J. Wetzel, K. Yi

Johns Hopkins University, Baltimore, USA

I. Anderson, B.A. Barnett, B. Blumenfeld, N. Eminizer, D. Fehling, L. Feng, A.V. Gritsan, P. Maksimovic, C. Martin, M. Osherson, J. Roskes, A. Sady, U. Sarica, M. Swartz, M. Xiao, Y. Xin, C. You

The University of Kansas, Lawrence, USA

P. Baringer, A. Bean, G. Benelli, C. Bruner, R.P. Kenny III, D. Majumder, M. Malek, M. Murray, S. Sanders, R. Stringer, Q. Wang

Kansas State University, Manhattan, USA

A. Ivanov, K. Kaadze, S. Khalil, M. Makouski, Y. Maravin, A. Mohammadi, L.K. Saini, N. Skhirtladze, S. Toda

Lawrence Livermore National Laboratory, Livermore, USA

D. Lange, F. Rebassoo, D. Wright

University of Maryland, College Park, USA

C. Anelli, A. Baden, O. Baron, A. Belloni, B. Calvert, S.C. Eno, C. Ferraioli, J.A. Gomez, N.J. Hadley, S. Jabeen, R.G. Kellogg, T. Kolberg, J. Kunkle, Y. Lu, A.C. Mignerey, Y.H. Shin, A. Skuja, M.B. Tonjes, S.C. Tonwar

Massachusetts Institute of Technology, Cambridge, USA

A. Apyan, R. Barbieri, A. Baty, K. Bierwagen, S. Brandt, W. Busza, I.A. Cali, Z. Demiragli, L. Di Matteo, G. Gomez Ceballos, M. Goncharov, D. Gulhan, Y. Iiyama, G.M. Innocenti, M. Klute, D. Kovalskyi, Y.S. Lai, Y.-J. Lee, A. Levin, P.D. Luckey, A.C. Marini, C. McGinn, C. Mironov, S. Narayanan, X. Niu, C. Paus, D. Ralph, C. Roland, G. Roland, J. Salfeld-Nebgen, G.S.F. Stephans, K. Sumorok, M. Varma, D. Velicanu, J. Veverka, J. Wang, T.W. Wang, B. Wyslouch, M. Yang, V. Zhukova

University of Minnesota, Minneapolis, USA

B. Dahmes, A. Evans, A. Finkel, A. Gude, P. Hansen, S. Kalafut, S.C. Kao, K. Klapoetke, Y. Kubota, Z. Lesko, J. Mans, S. Nourbakhsh, N. Ruckstuhl, R. Rusack, N. Tambe, J. Turkewitz

University of Mississippi, Oxford, USA

J.G. Acosta, S. Oliveros

University of Nebraska-Lincoln, Lincoln, USA

E. Avdeeva, K. Bloom, S. Bose, D.R. Claes, A. Dominguez, C. Fangmeier, R. Gonzalez Suarez, R. Kamalieddin, J. Keller, D. Knowlton, I. Kravchenko, F. Meier, J. Monroy, F. Ratnikov, J.E. Siado, G.R. Snow

State University of New York at Buffalo, Buffalo, USA

M. Alyari, J. Dolen, J. George, A. Godshalk, C. Harrington, I. Iashvili, J. Kaisen, A. Kharchilava, A. Kumar, S. Rappoccio, B. Roobahani

Northeastern University, Boston, USA

G. Alverson, E. Barberis, D. Baumgartel, M. Chasco, A. Hortiangtham, A. Massironi, D.M. Morse, D. Nash, T. Orimoto, R. Teixeira De Lima, D. Trocino, R.-J. Wang, D. Wood, J. Zhang

Northwestern University, Evanston, USA

K.A. Hahn, A. Kubik, N. Mucia, N. Odell, B. Pollack, A. Pozdnyakov, M. Schmitt, S. Stoynev, K. Sung, M. Trovato, M. Velasco

University of Notre Dame, Notre Dame, USA

A. Brinkerhoff, N. Dev, M. Hildreth, C. Jessop, D.J. Karmgard, N. Kellams, K. Lannon, N. Marinelli, F. Meng, C. Mueller, Y. Musienko³⁹, M. Planer, A. Reinsvold, R. Ruchti, G. Smith, S. Taroni, N. Valls, M. Wayne, M. Wolf, A. Woodard

The Ohio State University, Columbus, USA

L. Antonelli, J. Brinson, B. Bylsma, L.S. Durkin, S. Flowers, A. Hart, C. Hill, R. Hughes, W. Ji, K. Kotov, T.Y. Ling, B. Liu, W. Luo, D. Puigh, M. Rodenburg, B.L. Winer, H.W. Wulsin

Princeton University, Princeton, USA

O. Driga, P. Elmer, J. Hardenbrook, P. Hebda, S.A. Koay, P. Lujan, D. Marlow, T. Medvedeva, M. Mooney, J. Olsen, C. Palmer, P. Piroué, H. Saka, D. Stickland, C. Tully, A. Zuranski

University of Puerto Rico, Mayaguez, USA

S. Malik

Purdue University, West Lafayette, USA

V.E. Barnes, D. Benedetti, D. Bortoletto, L. Gutay, M.K. Jha, M. Jones, K. Jung, D.H. Miller, N. Neumeister, B.C. Radburn-Smith, X. Shi, I. Shipsey, D. Silvers, J. Sun, A. Svyatkovskiy, F. Wang, W. Xie, L. Xu

Purdue University Calumet, Hammond, USA

N. Parashar, J. Stupak

Rice University, Houston, USA

A. Adair, B. Akgun, Z. Chen, K.M. Ecklund, F.J.M. Geurts, M. Guilbaud, W. Li, B. Michlin, M. Northup, B.P. Padley, R. Redjimi, J. Roberts, J. Rorie, Z. Tu, J. Zabel

University of Rochester, Rochester, USA

B. Betchart, A. Bodek, P. de Barbaro, R. Demina, Y. Eshaq, T. Ferbel, M. Galanti, A. Garcia-Bellido, J. Han, A. Harel, O. Hindrichs, A. Khukhunaishvili, G. Petrillo, P. Tan, M. Verzetti

Rutgers, The State University of New Jersey, Piscataway, USA

S. Arora, A. Barker, J.P. Chou, C. Contreras-Campana, E. Contreras-Campana, D. Ferencek, Y. Gershtein, R. Gray, E. Halkiadakis, D. Hidas, E. Hughes, S. Kaplan, R. Kunnawalkam Elayavalli, A. Lath, K. Nash, S. Panwalkar, M. Park, S. Salur, S. Schnetzer, D. Sheffield, S. Somalwar, R. Stone, S. Thomas, P. Thomassen, M. Walker

University of Tennessee, Knoxville, USA

M. Foerster, G. Riley, K. Rose, S. Spanier, A. York

Texas A&M University, College Station, USA

O. Bouhali⁷⁰, A. Castaneda Hernandez⁷⁰, A. Celik, M. Dalchenko, M. De Mattia, A. Delgado, S. Dildick, R. Eusebi, J. Gilmore, T. Huang, T. Kamon⁷¹, V. Krutelyov, R. Mueller, I. Osipenkov, Y. Pakhotin, R. Patel, A. Perloff, A. Rose, A. Safonov, A. Tatarinov, K.A. Ulmer²

Texas Tech University, Lubbock, USA

N. Akchurin, C. Cowden, J. Damgov, C. Dragoiu, P.R. Duerdo, J. Faulkner, S. Kunori, K. Lamichhane, S.W. Lee, T. Libeiro, S. Undleeb, I. Volobouev

Vanderbilt University, Nashville, USA

E. Appelt, A.G. Delannoy, S. Greene, A. Gurrola, R. Janjam, W. Johns, C. Maguire, Y. Mao, A. Melo, H. Ni, P. Sheldon, B. Snook, S. Tuo, J. Velkovska, Q. Xu

University of Virginia, Charlottesville, USA

M.W. Arenton, B. Cox, B. Francis, J. Goodell, R. Hirosky, A. Ledovskoy, H. Li, C. Lin, C. Neu, T. Sinthuprasith, X. Sun, Y. Wang, E. Wolfe, J. Wood, F. Xia

Wayne State University, Detroit, USA

C. Clarke, R. Harr, P.E. Karchin, C. Kottachchi Kankanamge Don, P. Lamichhane, J. Sturdy

University of Wisconsin, Madison, USA

D.A. Belknap, D. Carlsmith, M. Cepeda, S. Dasu, L. Dodd, S. Duric, B. Gomber, M. Grothe, R. Hall-Wilton, M. Herndon, A. Hervé, P. Klabbbers, A. Lanaro, A. Levine, K. Long, R. Loveless, A. Mohapatra, I. Ojalvo, T. Perry, G.A. Pierro, G. Polese, T. Ruggles, T. Sarangi, A. Savin, A. Sharma, N. Smith, W.H. Smith, D. Taylor, N. Woods

†: Deceased

- 1: Also at Vienna University of Technology, Vienna, Austria
- 2: Also at CERN, European Organization for Nuclear Research, Geneva, Switzerland
- 3: Also at State Key Laboratory of Nuclear Physics and Technology, Peking University, Beijing, China
- 4: Also at Institut Pluridisciplinaire Hubert Curien, Université de Strasbourg, Université de Haute Alsace Mulhouse, CNRS/IN2P3, Strasbourg, France
- 5: Also at National Institute of Chemical Physics and Biophysics, Tallinn, Estonia
- 6: Also at Skobeltsyn Institute of Nuclear Physics, Lomonosov Moscow State University, Moscow, Russia
- 7: Also at Universidade Estadual de Campinas, Campinas, Brazil
- 8: Also at Centre National de la Recherche Scientifique (CNRS) - IN2P3, Paris, France
- 9: Also at Laboratoire Leprince-Ringuet, Ecole Polytechnique, IN2P3-CNRS, Palaiseau, France
- 10: Also at Joint Institute for Nuclear Research, Dubna, Russia
- 11: Also at Helwan University, Cairo, Egypt
- 12: Now at Zewail City of Science and Technology, Zewail, Egypt
- 13: Also at Beni-Suef University, Bani Sweif, Egypt
- 14: Now at British University in Egypt, Cairo, Egypt
- 15: Now at Ain Shams University, Cairo, Egypt
- 16: Also at Université de Haute Alsace, Mulhouse, France
- 17: Also at Tbilisi State University, Tbilisi, Georgia
- 18: Also at RWTH Aachen University, III. Physikalisches Institut A, Aachen, Germany
- 19: Also at Indian Institute of Science Education and Research, Bhopal, India
- 20: Also at University of Hamburg, Hamburg, Germany

- 21: Also at Brandenburg University of Technology, Cottbus, Germany
- 22: Also at Institute of Nuclear Research ATOMKI, Debrecen, Hungary
- 23: Also at Eötvös Loránd University, Budapest, Hungary
- 24: Also at University of Debrecen, Debrecen, Hungary
- 25: Also at Wigner Research Centre for Physics, Budapest, Hungary
- 26: Also at University of Visva-Bharati, Santiniketan, India
- 27: Now at King Abdulaziz University, Jeddah, Saudi Arabia
- 28: Also at University of Ruhuna, Matara, Sri Lanka
- 29: Also at Isfahan University of Technology, Isfahan, Iran
- 30: Also at University of Tehran, Department of Engineering Science, Tehran, Iran
- 31: Also at Plasma Physics Research Center, Science and Research Branch, Islamic Azad University, Tehran, Iran
- 32: Also at Laboratori Nazionali di Legnaro dell'INFN, Legnaro, Italy
- 33: Also at Università degli Studi di Siena, Siena, Italy
- 34: Also at Purdue University, West Lafayette, USA
- 35: Also at International Islamic University of Malaysia, Kuala Lumpur, Malaysia
- 36: Also at Malaysian Nuclear Agency, MOSTI, Kajang, Malaysia
- 37: Also at Consejo Nacional de Ciencia y Tecnología, Mexico city, Mexico
- 38: Also at Warsaw University of Technology, Institute of Electronic Systems, Warsaw, Poland
- 39: Also at Institute for Nuclear Research, Moscow, Russia
- 40: Now at National Research Nuclear University 'Moscow Engineering Physics Institute' (MEPhI), Moscow, Russia
- 41: Also at St. Petersburg State Polytechnical University, St. Petersburg, Russia
- 42: Also at INFN Sezione di Padova; Università di Padova; Università di Trento (Trento), Padova, Italy
- 43: Also at Faculty of Physics, University of Belgrade, Belgrade, Serbia
- 44: Also at INFN Sezione di Roma; Università di Roma, Roma, Italy
- 45: Also at National Technical University of Athens, Athens, Greece
- 46: Also at Scuola Normale e Sezione dell'INFN, Pisa, Italy
- 47: Also at University of Athens, Athens, Greece
- 48: Also at Institute for Theoretical and Experimental Physics, Moscow, Russia
- 49: Also at Albert Einstein Center for Fundamental Physics, Bern, Switzerland
- 50: Also at Adiyaman University, Adiyaman, Turkey
- 51: Also at Mersin University, Mersin, Turkey
- 52: Also at Cag University, Mersin, Turkey
- 53: Also at Piri Reis University, Istanbul, Turkey
- 54: Also at Gaziosmanpasa University, Tokat, Turkey
- 55: Also at Ozyegin University, Istanbul, Turkey
- 56: Also at Izmir Institute of Technology, Izmir, Turkey
- 57: Also at Marmara University, Istanbul, Turkey
- 58: Also at Kafkas University, Kars, Turkey
- 59: Also at Mimar Sinan University, Istanbul, Istanbul, Turkey
- 60: Also at Yildiz Technical University, Istanbul, Turkey
- 61: Also at Hacettepe University, Ankara, Turkey
- 62: Also at Rutherford Appleton Laboratory, Didcot, United Kingdom
- 63: Also at School of Physics and Astronomy, University of Southampton, Southampton, United Kingdom
- 64: Also at Instituto de Astrofísica de Canarias, La Laguna, Spain

- 65: Also at Utah Valley University, Orem, USA
- 66: Also at University of Belgrade, Faculty of Physics and Vinca Institute of Nuclear Sciences, Belgrade, Serbia
- 67: Also at Facoltà Ingegneria, Università di Roma, Roma, Italy
- 68: Also at Argonne National Laboratory, Argonne, USA
- 69: Also at Erzincan University, Erzincan, Turkey
- 70: Also at Texas A&M University at Qatar, Doha, Qatar
- 71: Also at Kyungpook National University, Daegu, Korea